Spring 4-30-2021

Serine and Glutathione Biosynthesis in Breast Cancer Subclones That Preferentially Metastasize to Lung and Bone

Noah Thornton

Serine and Glutathione Biosynthesis in Breast Cancer Subclones That Preferentially Metastasize to Lung and Bone

By
Noah Thornton

A thesis submitted to the faculty of The University of Mississippi in partial fulfillment of the requirements of the Sally McDonnell Barksdale Honors College.

Oxford, MS
May 2021

Approved By:

_____
Advisor: Dr. Mika Jekabsons

_____
Reader: Dr. Brian Doctor

_____
Reader: Dr. Carol Britson

ACKNOWLEDGEMENTS

First of all, I would like to thank Dr. Mika Jekabsons for his inspiring expertise, guidance, and patience throughout the last few years that are culminating with this project. The lessons of intellectual curiosity, conceptual understanding, and application of knowledge he has imparted on me will enhance my future research endeavors and career. I would also like to thank the Sally McDonnel Barksdale Honors College and the University of Mississippi Biology Department for providing me with the opportunities to pursue my passions. I also appreciate both Dr. Brian Doctor and Dr. Carol Britson for their time committed to this project. This would not have been possible without the hard work of Anna Skubiz, Mollie Merrell, and Blake Raboin. Lastly, many thanks to my friends and family for providing support and encouragement throughout my involvement in this project.

\

ABSTRACT

NOAH THORNTON: Serine and Glutathione Biosynthesis in Breast Cancer Subclones That Preferentially Metastasize to Lung and Bone
(Under the direction of Dr. Mika Jekabsons)

Metastatic breast cancers show distinct preferences to metastasize to lung and bone tissue. Transcriptomic analysis of lung-specific (LM) and bone-specific (BoM) subclones derived from the MDA-231 breast cancer line have identified differential expression of genes that may mediate this tissue-specific metastasis, but metabolic differences have not been systematically studied. If common metabolic phenotypes emerge in metastatic cancers having preferences for different organs, then such 'metabolic plasticity' may offer new therapeutic targets for treatment of specific metastases. Changes in glutathione (GSH) and serine synthesis may contribute to tissue-specific proliferation because of their roles in redox homeostasis, biosynthetic reactions including nucleotide synthesis, and/or energy metabolism. This study tests the hypothesis that glucose flux to serine, serine flux through the folate cycle, and glutamine flux to GSH differ between the parent MDA-231 breast cancer line, the LM and BoM lines, and the less malignant T47D breast cancer line. Using a combination of approaches including analysis of ^{13}C serine enrichment from [1,2-^{13}C] glucose by mass spectrometry and metabolic flux analysis, LM and BoM lines exhibited greater rates of serine synthesis than the T47D line, while there was no flux of glucose to serine in MDA-231 cells. Notably, LM and BoM serine synthesis was sufficiently high to negatively affect glycolysis, presumably through the NADH:NAD ratio. Folate cycle fluxes in LM and BoM lines were generally greater than those in T47D cells, as determined by metabolic flux analysis; these fluxes could not be determined in MDA-231 cells since glucose was not used to synthesize serine. LM cells exhibited no detectable GSH synthesis, while approximately 10% of the glutamine consumed by the other three lines was used for GSH synthesis, as determined by BSO-sensitive glutamine consumption. Higher glucose flux to serine in the BoM and LM lines are likely related to their higher proliferation rates rather

than their specificity for metastasis to bone or lung. The lack of BSO-sensitive glutamine consumption in LM cells was surprising, and implies that this cell line may rely more on peroxiredoxin and/or thioredoxin than GSH for redox homeostasis. Further studies with different lung and bone-specific cancer lines are necessary to determine if unique metabolic phenotypes exist for these metastatic cancers.

TABLE OF CONTENTS

LIST OF FIGURES AND TABLES

LIST OF ABBREVIATIONS

LM	Lung-specific metastatic breast cancer subclone
BoM	Bone-specific metastatic subclone
MDA-231	MDA-MB-231 metastatic breast cancer line
T47D	Control breast cancer line
GSH	Glutathione
OXPHOS	Oxidative Phosphorylation
ROS	Reactive Oxygen Species
TCA	Tricarboxylic Acid
3PG	3-phosphoglycerate
Glu	Glutamate
Gln	Glutamine
HxP	Hexose Phosphate
TrP	Triose Phosphate
PHGDH	Phosphoglycerate dehydrogenase
G6PDH	Glucose-6-phosphate dehydrogenase
ATP	Adenosine triphosphate
NADPH	Nicotinamide adenine dinucleotide phosphate
NADH	Nicotinamide adenine dinucleotide
EDC	Ethylcarbodilimide
AQC	6-Aminoquinolyl-N-hydroxysuccinimidyl
BSA	Bovine Serum Albumin

BSO	Buthionine sulfoximine
BCA	Bicinchoninic acid
LC-TQ MS	Liquid chromatography, triple quadrupole mass spectrometry
GSSG	Glutathione Disulfide
Gpx	Glutathione Peroxidase
Grx	Glutaredoxin
FAK	Focal Adhesion Kinase
SHMT-2	Serine hydroxymethyltransferase-2
mTHF	methyl-tetrahydrofolate
BrM	Brain metastatic breast cancer subclone
DHAP	Dihydroxyacetone-phosphate

Introduction

Cancer is characterized by unregulated cell growth and proliferation, and altered fluxes through a number of metabolic pathways involved in energy production and biosynthetic processes necessary to support this phenotype (1, 2). However, unique metabolic signatures associated with heterogeneity of the tumor microenvironment within an organ (e.g., regional differences in hypoxia within a solid tumor) or, in the case of metastatic cancers, between different organs (e.g., differences in mass-specific blood flow and/or metabolism of each organ) are known to occur (3, 4). Reprogramming of cancer metabolism either during cancer progression or metastasis, a concept known as metabolic plasticity, may facilitate tumorigenesis or preferential metastasis to a specific organ (5). The triple-negative breast cancer cells (no expression of estrogen receptor, progesterone receptor, or human epithelial receptor 2), MDA-MB-231, have a different metabolic phenotype upon intravasation, indicating that the relatively few cells leaving the primary tumor may have differing metabolic properties from the majority of cells within the primary breast tumor (5). The environment in which cancer cells reside may provide selective pressures, such as limited availability of select nutrients or variations in oxygen and/or carbon dioxide content, that either drive metabolic adaptations or determine which subset of metabolically aberrant cells successfully metastasize to a specific secondary organ (6). Irrespective of whether metabolic plasticity is a stochastic process driven by genomic instability in proliferating cells within the primary tumor or by selective pressures after invasion of a secondary organ, an understanding of the specific metabolic signatures of tumor sub-clones that preferentially invade a specific organ is required to identify potential targets for the development of organ-specific metastasis therapies.

Transcriptomic profiling has shown that sub-clones of metastatic tumors that preferentially invade different organs have different gene expression profiles (7). Therefore, individual cells within the MDA-MB-231 metastatic breast cancer line are genetically heterogeneous. This heterogeneity contributes to the probability of specific metastasis to the lungs, bone, or brain by MDA-MB-231 cells (8). Experiments

using bioluminescence imaging have revealed that MDA-MB-231 cells isolated from the lungs, bones, or brain and then expanded in vitro, exhibit a high probability of selectively invading the same organ from which they were derived following re-injection into the circulatory system of nude mice (7). The isolation of highly lung-, bone-, and brain-specific metastatic subclones from the parent MDA-MB-231 line has provided insight on genes that contribute to organ specific metastasis. Breast cancers that metastasize to the lungs over-express 50 genes that are directly and almost exclusively correlated with lung metastasis (9 & 10). Similarly, there are many genes unique to bone-specific metastasis, with limited overlap between the genes that support the invasion of bone and lung tissue (9, 11). Breast cancer cells have been proven to require specialized function, potentially mediated through gene expression, in order to colonize in brain tissue, furthering the point of tissue-specific, varied environments giving rise to different metastatic speciations as well (9). Although the majority of these genes have a role in cell signaling, proliferation, and immune responses, the transcriptomic analysis was incomplete so the role of metabolic genes in this process remains unclear.

Common metabolic changes among cancer cells arise from de-regulated anabolic pathways, glycolysis, and the uptake of nutrients; glucose and glutamine are the two primary nutrients which support survival and biosynthesis. The Warburg effect, discovered by Otto Warburg, details that even in the presence of oxygen, cancer cells metabolize glucose to lactate at extremely high rates, as opposed to the complete oxidation of glucose to carbon dioxide by the more efficient ATP production mechanism of oxidative phosphorylation (OXPHOS; 1). This effect, also known as aerobic glycolysis, is thought to increase the supply of glycolytic intermediates, which may be used in myriad of biosynthesis pathways (Fig. 1). Beyond these difference with untransformed cells, there is often notable variation of metabolic pathways within different cancers. Although glucose and glutamine are important for growth in most cancer cells, the fraction used by each anabolic pathway may vary depending on the local microenvironment in which the cancer cells reside. For example, the fraction of glucose used by the pentose phosphate pathway, fatty acid synthesis, serine synthesis, or oxidation by the mitochondria can vary depending on reactive oxygen species (ROS) production, availability pf biosynthetic substrates, ATP demand, uptake capacity of fatty

acids, and mitochondrial function. Similarly, glutamine used for protein, glutathione, or fatty acid synthesis, and for oxidation by the tricarboxylic acid (TCA) cycle and/or malic enzyme can vary depending on ROS production and availability of other substrates. Therefore, transcriptomic changes, energy demands, as well as prevailing microenvironment conditions likely play a role in the metabolic adaptations metastatic cancer cells develop as they progress from the parent tumor to their secondary sites of metastasis (12).

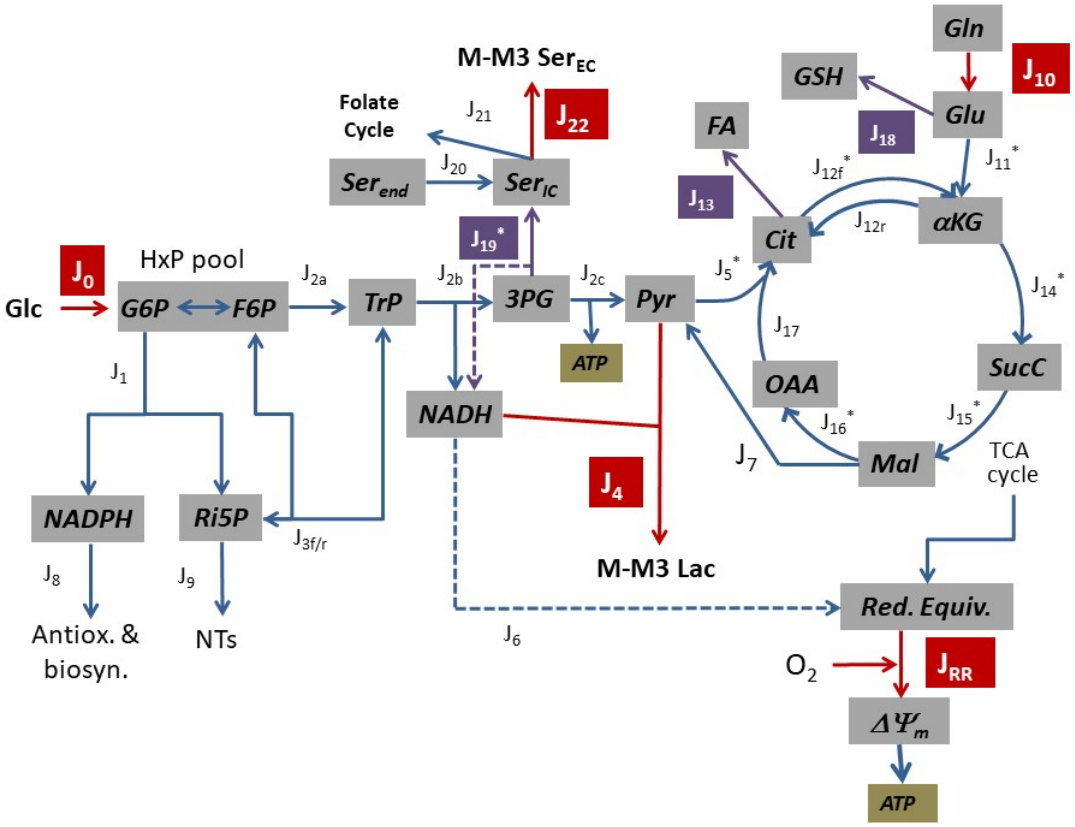

Figure 1: *A simplified map of cancer metabolism, including glycolysis and the tricarboxylic acid cycle (TCA). The experiments in the current study are part of a larger set of experiments designed to quantify fluxes through all the indicated reactions. The reactions are linked together through the shared intermediates indicated by grey boxes. Fluxes highlighted in red and purple are measured; all other fluxes are inferred. For the current study, the objective was to determine fluxes from 3-phosphoglycerate (3PG) to serine (J_{19}), and glutamate (Glu) flux the glutathione (GSH). Cells were given [1,2-^{13}C] glucose, and ^{13}C enrichment in serine (M-M3) and lactate (M-M3) and serine export from the cells (J_{22}) determined to quantify J_{19} and folate cycle fluxes (J_{21} and other fluxes not shown) by computational modeling. Measurements of glucose uptake (J_0), lactate production (J_4), and mitochondrial respiration (J_{RR}) provided constraints in the model. Pharmacological inhibition of GSH synthesis with buthionine sulfoximine was used to assess J_{18} by reduction in glutamine (Gln) uptake (J_{10}).*

Enhanced aerobic glycolysis and glucose uptake in part reflect the importance of glycolysis for de-novo synthesis of nucleotides, amino acids, lipids, and reducing equivalents such as NADPH, all of which are

necessary for cell proliferation (4). Cancer cell proliferation is controlled by the availability of ATP as well as multiple intermediates that serve as substrates for the synthesis of lipids, nucleic acids, and proteins necessary to bolster the expanding biomass (13). Specifically, the oxidative and non-oxidative pentose phosphate pathways (J_1 and $J_{3f/r}$ in Fig. 1) are responsible for providing pentose sugars for the biosynthesis of nucleic acids, and it is directly connected to glycolysis through the hexose phosphate (HxP; glucose-6-phosphate and fructose-6-phosphate) and triose phosphate (TrPs; glyceraldehyde-3-phosphate and dihydroxyacetone phosphate) pools. Similarly, glycolysis produces 3-phosphoglycerate, which is a key cellular intermediate towards synthesis of various amino acids, such as serine and glycine, as well as purine nucleotides through one carbon metabolism in the folate cycle (12). The folate cycle produces glycine and cysteine, which are components of GSH, through re- and de-methylation reactions, purine units, necessary for nucleotide and ATP/GTP generation, and NADPH, involved in redox regulation. Serine is a major donor of one-carbon units into the folate cycle, making it implicated in these biosynthetic processes (14). The de-novo synthesis of serine from 3PG is initiated by the enzyme phosphoglycerate dehydrogenase (PHGDH), which has been implicated in cancer progression and/or metastasis due to its elevated expressions in some cancers (15). Cancer cells must synthesize nucleotides at a high rate for continued replication of the genome, and thus require a steady supply of glycolytic intermediates that can be used in the biosynthetic pathways that fuel their growth and proliferation (4). One focus of the current study is to assess potential differences in serine synthesis and folate cycle fluxes in breast cancer subclones preferentially metastasizing to lung or bone tissue.

Similarly, increased glutaminolysis, the breakdown of glutamine into various metabolites, is a trademark feature of cancer cells, which supports the need for increased glutamine uptake in cancer cells (16). Glutamine is deaminated to glutamate and subsequently oxidized to α-ketoglutarate, a TCA cycle intermediate which contributes to ATP production and synthesis of fatty acids and cytochromes (16). DNA synthesis is constrained by glutamine availability in some cancers, reinforcing the idea of glutamine as an obligate nitrogen donor for purine and pyrimidine synthesis for nucleotides (16). Fatty acid

synthesis, necessary for the production of new cell membranes, is also fueled by glutamine through α-ketoglutarate and subsequent reductive carboxylation to citrate (3). Lastly, glutamine, through conversion to glutamate, is also used in the de-novo synthesis of glutathione, an endogenous antioxidant (16).

Redox homeostasis, the balance of reactive oxygen species (ROS) levels, plays an important role in cell survival (3). ROS are intracellular chemical species that, when at high levels causing oxidative stress, become exceedingly lethal by damaging DNA, proteins, and lipids. (17). The high aerobic glycolysis flux coupled with low mitochondrial activity that characterizes many cancers are conditions that may promote elevated ROS levels, which can induce oxidative stress (18). Moreover, breast cancer sub-clones that preferentially metastasize to lung may be subjected to greater oxidative stress and thus have a greater demand for glutathione. However, at low levels, ROS have been shown to oxidize cysteineresidues in various proteins to induce proliferative signals (3). Antioxidants, such as glutathione (GSH), serve as a cofactor in reactions catalyzed by glutathione peroxidase and glutaredoxin that, respectively, reduce hydrogen peroxide to water and maintain protein thiols in their reduced state. A second focus of the current study is to determine if GSH synthesis from glutamine differs between breast cancer sub-clones that preferentially metastasize to lung and bone.

Breast cancer sub-clones that preferentially metastasize to lung or bone tissue (designated LM and BoM cells, respectively) exhibit greater proliferation rates than the parent MDA-231 cells and the less malignant T47D breast cancer line. Such differences suggest the demand for nucleotides and amino acids differ among these lines. Furthermore, differences in the partial pressure of oxygen within the microenvironments preferred by these lines suggests potential their capacities for antioxidant defenses may vary. This study aims to quantify fluxes through the pathways that synthesize serine and GSH as well as the folate cycle. We hypothesize that the more proliferative BoM sub clone will exhibit greater serine biosynthesis from glucose than the LM, parent MDA-231, and less malignant T47D lines because of the limited blood flow, and hence serine supply, to bone tissue. LM and BoM lines are hypothesized to exhibit greater flux of serine into the folate cycle to support their higher proliferation rates than the MD-

231 and T47D lines. Additionally, LM cells are hypothesized to exhibit a higher flux of glutamine to GSH because of the potentially more oxidizing environment of the lungs.

Methods

A. Materials

Glutamate pyruvate transaminase, glucose-6-phosphate dehydrogenase (G6PDH), lactate dehydrogenase, oxidized and reduced forms of nicotinamide adenine dinucleotide phosphate (NADP(H)), adenosine triphosphate (ATP), and 2-oxoglutarate were purchased from Calzyme (San Luis Obispo, CA). Hexokinase, microbial glutamate dehydrogenase, N-(3-dimethylaminopropyl)-N'-ethylcarbodiimide (EDC), 3-nitrophenylhydrazine (NPH), buthionine sulfoximine (BSO), and CBR-5884 were purchased from Sigma (St. Louis, MO). 6-Aminoquinolyl-N-hydroxysuccinimidyl Carbamate (AQC) was purchased from Toronto Research Chemicals (Toronto, Canada). Glutaminase was purchased from Megazyme (Chicago, IL). [1,2] ^{13}C glucose was purchased from Cambridge Isotopes (Tewksbury, MA). Cell culture media, fetal bovine serum, and cell culture supplies were purchased from Fisher Scientific (Pittsburg, PA). Buffers and other general reagents were purchased from Sigma (St. Louis, MO)

B. Cell lines

Metastatic breast cancer MDA-MB-231 cells (hereafter referred to as MDA-231) and the less aggressive T47D breast cancer cells were provided by Dr. Y.D. Zhou (University of Mississippi, Department of Chemistry and Biochemistry). Sub-clones of MDA-231 cells that preferentially metastasize to lung (LM) and bone (BoM) were generated by Massague's lab (10,11). Both LM and BoM cells were obtained from Dr. Kounosuke Watabe (Wake Forest University) and provided by Dr. Zhou. Cells were routinely cultured using RPMI-1640 media supplemented with 10% fetal bovine serum and 0.5% vol/vol penicillin-streptomycin in 10 cm polystyrene petri dishes at 37^{o}C in a humidified 5% CO_2 incubator. Cells were maintained in culture for no more than 20 passages, and typically split twice a week.

C. Pharmacological Experiments with BSO and CBR-5884

Cells were seeded in 2-well Lab-Tek II chambers (0.9-1.2 x 10^6 cells per well) and maintained at 37°C/5% CO_2 in RPMI medial supplemented with 10% fetal bovine serum and 0.5% penicillin/streptomycin one day prior to experiments. Cells were washed in experimental buffer containing 137 mM NaCl, 5 mM KCl, 20 mM TES, 1.3 mM $CaCl_2$, 1.3 mM $MgCl_2$, 1.2 mM Na_2SO_4, 0.4 mM KH_2PO_4, 0.2 mM $NaHCO_3$, 5.5 mM glucose, 0.3 % fatty acid-free bovine serum albumin (BSA), 1.5 mM glutamine, pH 7.4 (hereafter referred to as experimental buffer). supplemented with 50 μM BSO or 40 μM CBR-5884; control buffers were supplemented with water (for BSO) or DMSO (for CBR-5884) as vehicle. For some CBR-5884 experiments, glutamine was omitted from the buffer. The cells were equilibrated at 37 °C for 2 hr (BSO) or 2.5 hr (CBR-5884) to allow for inhibition of de-novo glutathione or serine synthesis, respectively. Cells were washed once then serially incubated with 350 μL at 37°C for 1 x 60, 1 x 120, 1 x 60 minutes (for BSO) or 3 x 60 min (for CBR-5884). Control wells without cells were run in parallel to account for changes in buffer concentrations of glucose and glutamine by evaporation. The buffer samples were centrifuged for 5 min, 21,000 xg, at 4°C to remove any cells. The supernatant was then stored at -20°C for analysis of glucose and glutamine. Following the final incubation, cells were washed once with 1 mL of Phosphate Buffered Saline (PBS) and then solubilized with 20 mM TES pH 7.3, 50 mM NaCl, and 1% SDS for 15 min at 37°C. The extracts were vortexed vigorously for 2 min, and then centrifuged for 10 min, 21,000 xg, at 10°C. The supernatants were stored at -20°C for analysis of total protein content.

D. Experiments with [1,2-^{13}C] glucose

Cells were seeded in 2-well Lab-Tek II chambers (0.9-1.2 x 10^6 cells per well) and maintained at 37oC/5% CO_2 in RPMI media supplemented with 10% fetal bovine serum and 0.5% penicillin/streptomycin one day prior to experiments. For each experiment, either T47D and MDA-231 cells or LM and BoM cells were seeded in separate wells of the chamber. The cells were washed once in 137 mM NaCl, 5 mM KCl, 20 mM TES pH 7.4, 1.3 mM $CaCl_2$, 1.3 mM $MgCl_2$, 1.2 mM Na_2SO_4, 0.4 mM KH_2PO_4, 0.2 mM $NaHCO_3$, 5.5 mM [1,2-^{13}C] glucose, and 0.3 % fatty acid-free bovine serum albumin (hereafter referred to as ^{13}C experimental buffer) then incubated in 1000 µl of ^{13}C experimental buffer for 5 h at 37^{o}C to allow glycolytic and TCA cycle metabolites to reach steady-state isotopic labeling; buffer was exchanged once during the equilibration period. Respiration rate of each well was measured at 37^{o}C in 2.15 ml of fresh ^{13}C experimental buffer using a Clark-type micro-oxygen electrode (Microelectrodes, Inc., Bedford, MA) positioned above the chamber with a custom-made lid. The oxygen concentration in each well was acquired over 45-55 min. with a Powerlab A/D unit and Lab Chart software. In total the cells were pre-equilibrated for approximately 6.5 h prior to incubations for assessing ^{13}C enrichment in serine and lactate. Cells were washed once then incubated for 2 x 60 min intervals at 37^{o}C with 350 µl experimental buffer; after the first interval, cells were washed once and given fresh buffer. Control wells without cells were run in parallel to correct for evaporation over each incubation interval. Buffer samples were centrifuged 5 min, 4^{o}C and 21,000 xg; the supernatants were stored at -20^{o}C for analysis of ^{13}C enrichment in extracellular lactate and serine.

E. Lactate derivatization and mass spectrometry analysis

The samples and M/M1 lactate standards prepared in experimental buffer (18 µL) were extracted with 2 volumes 100% cold methanol and then incubated for 1 h at -20°C to precipitate buffer proteins. The samples were centrifuged at 21,000 xg, 2°C for 10 min. The supernatants (54 µL) were derivatized by incubation with 27 µL50 mM N-(3-dimethylaminopropyl)-N'-ethylcarbodiimide (prepared fresh in 1.5% pyridine, 98.5% ethanol) and 27 µl 140 mM 3-nitrophenylhydrazine (prepared fresh in 50% ethanol) for 2 h at 37°C, cooled on ice, then diluted 1:50 in mass spec vials with 80% methanol for analysis by liquid

chromatography-triple quadrupole mass spectrometry. Both unlabeled (M), ^{13}C labeled (M1), and 66:1 M:M1 mixed lactate standards were run to confirm the expected masses (224 Da for M, 225 Da for M1) and verify separation of these isotopologues.

The derivatized samples were separated on a Waters ACQUITY I-Class UPLC™ system including binary solvent manager, sample manager and column manager connected to a Waters Xevo TQ-S triple quadrupole mass spectrometer (Waters Corp, Milford, MA, USA). The separation was carried out on a Waters Acquity UPLC™ BEH C18 column (50mm × 2.1mm i.d., 1.7 µm). The sample temperature and column temperature were maintained at 10 °C and 40 °C, respectively. The mobile phase consisted of water containing 0.1% formic acid (v/v) (A) and acetonitrile with 0.1% formic acid (B). The analysis was performed using the following gradient elution at a flow rate of 0.50 mL/min: 0-2.5 min, 5% B to 18% B; 2.5-3 min, 18% B to 100% B. Each run was followed by a 2.5 min wash with 100% B and an equilibration period of 2.5 min with the initial conditions. The strong and weak solutions used to wash the auto sampler were methanol/acetonitrile/isopropanol/water (25:25:25:25, v/v/v/v/v) and methanol/water (70:30, v/v), respectively. The injection volume was 1 µl. The UHPLC effluent was introduced into the Waters Xevo TQ-S mass spectrometer equipped with electrospray ionization in negative ion mode (ESI-) for quantification of the analytes. Detection was obtained by Multiple Reaction Monitoring (MRM) mode including two MRMs for confirmation of the analytes. MRM transitions and related parameters are listed in Table 1. The quantification of analytes 224, 225, 226, and 227 (the expected masses for M, M1, M2, and M3 lactate derivatized with nitrophenylhydrazine, respectively) was acquired with transitions of deprotonated ion at *m/z* 224.04 → 152.06 for M, 225.04 → 152.06 for M1, 226.04 → 152.06 for M2, and 227.04 → 152.06 for M3 with dwell time of 20 msec at cone voltage 44 V and collision energy 14 eV for each transition. The ESI–MS/MS parameters were set as follows: capillary voltage, 1.20 kV; cone voltage, 44 V; source temperature, 150 °C; desolvation temperature, 600 °C; desolvation gas flow, 600 L/h, cone gas flow, 200 L/h. Nitrogen was used as desolvation and cone gas. Argon (99.99% purity) was introduced

as the collision gas into the collision cell at a flow rate of 0.15 mL/min. Data acquisition was carried out by MassLynx 4.1 software and processed by TargetLynx (Waters Corp., Milford, MA, USA).

Table 1: Optimized UHPL-MS/MS parameters for each analyte

Analyte	$[M-H]^-$ (*m/z*)	MRM transition (*m/z*)	Cone voltage (V)	Collision energy (eV)	Retention time (min)
M	224.04	224.04 -> 152.06	44	14	1.84
		224.04 -> 137.11		22	
M1	225.04	225.04 -> 152.06	44	14	1.84
		225.04 -> 137.11		22	
M2	226.04	226.04 -> 152.06	44	14	1.84
		226.04 -> 137.11		22	
M3	227.04	227.04 -> 152.06	44	14	1.84
		227.04 -> 137.11		22	

F. Serine Derivation and Mass Spectrometry Analysis

The samples and serine standards in experimental buffer (20 µL) were extracted with 10 µL of 0.6 M trichloroacetic Acid (TCA) for 30 min on ice and then centrifuged for 10 min, 21,000xg, at 4℃. An aliquot of the supernatant (12 µL) was neutralized with 36 µL of sodium borate (pH = 9.3). Stock 10 mM

AQC was prepared fresh in anhydrous acetonitrile by incubating for 10 min at 55℃. Primary and secondary amines in the neutralized samples were derivatized with 24 µL 10mM AQC for 10 min at 55℃.

F.1. Serine Mass Spectrometry Analysis

All analysis was performed on a Waters ACQUITY I-Class UPLC™ system coupled with a Waters Xevo TQ-S triple quadrupole mass spectrometer (Waters Corp, Milford, MA, USA). A Waters Acquity UPLC BEH C18 column (50 mm × 2.1 mm I.D., 1.7 µm) was used with a mobile phase composed of water containing 0.1 % formic acid (A) and acetonitrile with 0.1 % formic acid (B). Sample and column temperatures were maintained at 10 °C and 40 °C, respectively. The LC flow rate was 0.35 mL/min in a gradient elution as follows: 0-1.5 min, 2% B to 20% B; 1.5-2.0 min, 20% B to 100% B. Each run was followed by a 2 min wash with 100% B and an equilibration period of 3 min with the initial conditions. The wash and purge solvents used to wash the autosampler were methanol/acetonitrile/isopropanol/water (25:25:25:25, v/v/v/v) and methanol/water (50:50, v/v), respectively. The effluent is directly guided into Xevo TQ-S mass spectrometer equipped with electrospray ionization in a positive ion mode (ESI+). Multiple Reaction Monitoring (MRM) mode including two MRMs for each analyte were used for quantification and confirmation respectively. MRMs of analytes 276, 277, 278, and 279 (the expected masses for M, M1, M2, and M3 of serine derivatized with AQC respectively; all had 1.08 min retention time) were recorded. For quantification of serine AQC derivatives, MRM transitions of protonated ion use at *m/z* 276.05 > 171.06 for M, 277.05 > 171.06 for M1, 278.05 > 171.06 for M2, and 279.05 > 171.06 for M3. The dwell time was 6 ms for each transition at cone voltage 46 V and collision energy 46 eV. The ESI+ MS/MS parameters were set as follows: capillary voltage, 2.50 kV; cone voltage, 38 V; source temperature, 150 °C; desolvation temperature, 500 °C; desolvation gas flow, 1000 L/h, cone gas flow, 150 L/h. Nitrogen was used as desolvation and cone gas. Argon (99.99% purity) as the collision gas was introduced into the collision cell at a flow rate of 0.15 mL/min. Data acquisition was carried out with MassLynx 4.1 software (Waters Corp., Milford, MA, USA).

F. Protein Assay

Determination of protein content in cell extracts (duplicates, diluted 1:3 in water) were determined by bicinchoninic acid (BCA) assay. 500 µL of BCA Reagent was added to 25 µL of diluted sample, and the reaction incubated for 30 min at 60℃, then cooled to room temperature before being quantitated at a 562 nm wavelength using a Ultrospec 3100pro spectrophotometer (Amersham Bioscience). 562 nm wavelength was used as the BCA reagent utilizes the reduction of Cu^{2+} to Cu^{1+} by protein, as BCA reacts with the reduced cation through chelation to form a BCA-Copper complex with a strong absorbance at 562 nm, which increases as protein concentration increases. Bovine Serum Albumin (BSA) standards (0, 50, 100, 150, 200, 300, 400, and 500 µg/ml) were dissolved in the same solubilization buffer as to prepare cell extracts and run alongside the test samples as standards of known protein content.

G. Metabolite Assays

G.1. Glucose Assay

The concentration of glucose remaining in the experimental buffer after incubation with cells was determined by enzymatic assay, and these concentrations were used to calculate glucose uptake rates. The samples and standards (5µl, in triplicate sets) were added to 115 µl of a reaction containing 100 mM triethanolamine pH 7.3, 7 mM $MgCl_2$, 2mM ATP, 2 mM NADP, 1U/mL glucose-6-phosphate dehydrogenase, and 1 U/mL hexokinase. Hexokinase and ATP catalyze the phosphorylation of glucose to glucose-6-Phosphate, which is then oxidized by glucose-6-phosphate dehydrogenase concomitant with the reduction of NADP to NADPH, the latter of which is fluorescence. The samples were incubated 10 min and the fluorescence was quantitated with a Shimadzu RF-6000 spectrofluoremeter (Ex=341 nm, Em=464 nm). Glucose standards (3.5, 4.0, 4.5, 5.0, 5.5, 6.0 mM) were run in the same buffer alongside the test samples, providing data used to create a linear regression to apply to the fluorescence seen in the test samples.

G.2. Glutamine Assay

The concentration of glutamine in the experimental buffer after incubation with cells was determined by a two-step enzymatic reaction. The samples and standards (6µl, in duplicate) were added to 34µl of buffer, containing 60 mM sodium acetate pH 4.5, and with or without 1 U/mL glutaminase. The glutaminase was added to cleave the amino group from glutamine, resulting in free ammonia and glutamate; control reactions without glutaminase were to assess background free ammonia in the samples. The duplicate samples were then incubated for 45 minutes at 37℃. The second enzymatic reaction as initiated by addition of 80µl reaction buffer containing 300 mM Tris pH 8.5, 10 mM 2-oxoglutarate, 240 µM NADPH, and 2 U/mL glutamate dehydrogenase. The addition of glutamate dehydrogenase uses the free ammonia, generated via glutaminase, to reductively aminate 2-oxoglutarate to Glutamate, subsequently oxidizing NADPH, the fluorescent target, to NADP. These mixtures were then incubated in the dark for 80 min at room temperature, (approximately 20-25°C). Following the second incubation, the fluorescence of the duplicate samples were quantified using the Shimadzu RF-6000 spectrolfluorophotometer (ex=341 nm, em=464 nm). Naturally occurring ammonia was controlled for by running the glutamine standards (0, 0.2, 0.4, 0.8, 1.2, 1.6, and 2.0 mM) without the presence of glutaminase, allowing us to subtract the fluorescence of NADPH of the cell samples from the standards.

H. Folate Cycle Flux Calculations

The folate cycle model (the basis for this model is in Figs. 1 and 5) has seven fluxes ($J_{19} – J_{25}$), one of which (J_{22}) is measured from LC-TQ mass spectrometry of serine. Three flux ratios are optimized by the model to reproduced the measured ^{13}C serine labeling pattern:

$$\frac{J_{19}}{J_{19}+J_{20}} = X \quad \text{(Eq. 1)}$$

$$\frac{J_{21}}{J_{21}+J_{24}} = Y \quad \text{(Eq. 2)}$$

$$\frac{J_{25}}{J_{19}+J_{25}} = Z \quad \text{(Eq. 3)}$$

The BSO-sensitive glutamine uptake rate (Fig. 2), which together with the ratio of average glutamine to glucose uptake (J_{10}^{avg}/J_0^{avg}) from experiments with [5-^{13}C] glutamine (unpublished) and the measured rate of [1,2-^{13}C] glucose uptake (J_0), were used to calculate a minimal estimate of cellular glycine consumption (J_{23}):

$$J_{23} = \frac{J_{10}^{cntl} - J_{10}^{BSO}}{J_{10}^{cntl}} * \frac{J_{10}^{avg}}{J_0^{avg}} * J_0 \quad \text{(Eq. 4)}$$

This approach assumes that the glutamine demand normalized to glucose uptake without exogenous glutamine (experiments with [1,2-^{13}C] glucose) is the same as that for cells given 1.5 mM [5-^{13}C] glutamine. With metabolic steady-state conditions, then the serine balance is:

$$J_{19} + J_{20} = J_{22} + J_{21} - J_{25} \quad \text{(Eq. 5)}$$

Substituting for J_{25} into Eq. 5 using Eq. 2:

$$J_{19} + J_{20} = \frac{J_{22} + J_{21}}{1+Z} \quad \text{(Eq. 6)}$$

The glycine balance is given as:

$$J_{21} + J_{24} = J_{23} + J_{25} \quad \text{(Eq. 7)}$$

Substituting for $J_{21} + J_{24}$ in Eq. 6 with J_{21}/Y from Eq. 2, and solving for J_{25}:

$$J_{25} = \frac{J_{21}}{Y} - J_{23} \quad \text{(Eq. 8)}$$

Substituting Eq. 6 and Eq. 8 into Eq. 5 and solving for J_{21}:

$$J_{21} = \frac{{}^{J_{22}}/_{(1+Z)} - J_{22} - J_{23}}{(1 - {}^{1}/_{Y}) - ({}^{1}/_{(1+Z)})} \quad \text{(Eq. 9)}$$

Then from Eq. 2:

$$J_{24} = \frac{1-Y}{Y} * J_{21} \quad \text{(Eq. 10)}$$

So from Eq. 6:

$$J_{25} = J_{21} + J_{24} - J_{23} \quad \text{(Eq. 11)}$$

Substituting the expression for $J_{19} + J_{20}$ in Eq. 5 into Eq. 1, then:

$$J_{19} = X * (J_{22} + J_{21} - J_{25}) \quad \text{(Eq. 12)}$$

$$\text{and } J_{20} = J_{22} + J_{21} - J_{25} - J_{19} \quad \text{(Eq. 13)}$$

For cells lacking BSO-sensitive glutamine uptake (LM line; see Fig. 2), J_{19} was estimated as that necessary to support J_7 (by production of NADH) so that the error between the measured

and model-calculated ^{13}C lactate labeling patterns was minimized (see Tables 2 and 3). Rearranging Eq. 1, then:

$$J_{20} = \frac{1-X}{X} * J_{19} \quad \text{(Eq. 14)}$$

From Eq. 3:

$$J_{25} = Z * (J_{19} + J_{20}) \quad \text{(Eq. 13)}$$

The remaining fluxes were determined using the relationships described in Eq. 5, Eq. 10, and Eq. 7.

Results

A. Glutamine used for de-novo glutathione biosynthesis.

Many tumor cells have elevated proliferation rates, and glutathione (GSH), a potent antioxidant and cell proliferation modulator, is associate with increased proliferation rates (19). Buthionine sulfoximine (BSO) is a synthetic amino acid analog that specifically inhibits gamma-glutamylcysteine synthetase, which is the enzyme that catalyzes the initial step of de-novo glutathione biosynthesis by converting L-glutamate to gamma-glutamyl cysteine, a precursor to glutathione (20). For these experiments in which the buffer was not supplemented with glutamate, exogenous glutamine is a significant source of glutamate through a deamination reaction catalyzed by the mitochondrial localized enzyme glutaminase. Therefore, BSO is expected to reduce glutamine demand and thus its uptake from the extracellular media for cells actively synthesizing GSH. This BSO-sensitive glutamine consumption thus provides a lower-limit estimate of GSH biosynthesis (Fig. 1, flux J_{18}). Pre-treatment for 2 h with BSO significantly reduced glutamine uptake rate measured over two one-hour intervals in the MDA-231 and BoM lines, and tended to reduce uptake in T47D cells ($p=0.107$), but was without effect in the LM line (Fig. 2A). The BSO-sensitive fraction of glutamine consumption was similar for MDA-231, BoM, and T47D lines (10.2±2.1, 8.8±3.4, and 13.5±7.3%, respectively; Fig. 2B); while there was no significant main effect of cell line on BSO-sensitive glutamine consumption (1-way ANOVA $p=0.292$), likely because of the low number of replicate experiments, the LM line notably differed with no indication of glutamine consumption for GSH synthesis.

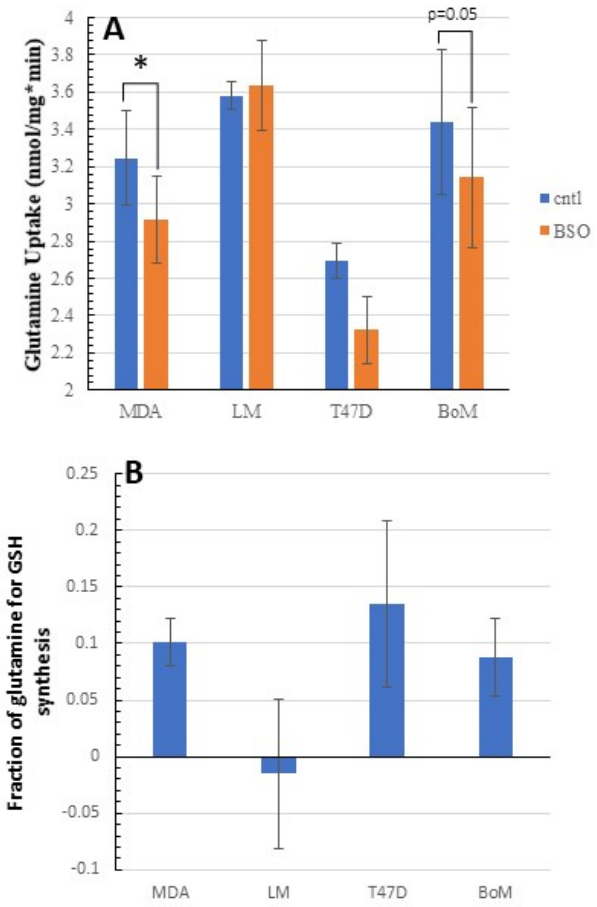

Figure 2: *BSO Sensitive Glutamine uptake rates (A) and fractional glutamine uptake for glutathione biosynthesis (B). Cell lines were pre-incubated in the presence or absence of 50 μM BSO for 2 h. The buffer glutamine concentrations were determined by enzymatic assay and the rates of uptake were averaged over two 60 min incubation periods. The rates were then normalized to total SDS-soluble protein. The data is presented as the mean ± standard error (n =3). Flux data in (A) were analyzed by one-tailed T-test and fractional uptake in (B) by 1-way ANOVA. Asterisks indicate a significant effect ($p<0.05$) of BSO.*

B. Glucose Uptake to assess de-novo serine biosynthesis

Glucose is a substrate used by tumor cells for a variety of homeostatic pathways, including energy through ATP synthesis, production of NADPH and NADH, and various anabolic processes, such as amino acid and nucleotide synthesis. Serine, which can be synthesized from glucose or obtained from the extracellular fluid, is an important amino acid necessary for protein synthesis, a source of glycine, as well as substrate for one-carbon metabolism in the folate cycle that is used for synthesis of purine nucleotides. The first step in de-novo serine biosynthesis is catalyzed by 3-phosphoglycerate dehydrogenase (PHGDH), the rate limiting enzyme that oxidizes 3-phosphoglycerate, a glycolytic intermediate, into phosphohydroxypyruvate, a precursor for serine with the concomitant reduction of NAD to NADH (13).

Two further steps convert phosphohydroxypyruvate to serine, with glutamate being a required co-substrate for the reaction catalyzed by phosphoserine aminotransferase. PHGDH is an NAD-dependent dehydrogenase that has been shown to be upregulated in some tumor cells and inhibited non-competitively by CBR-5884 (14, 21). For cancer cells synthesizing serine, demand for 3PG, and correspondingly supply of this substrate by glucose consumption through glycolysis, are predicted to decrease upon inhibition by CBR-5884; thus, the CBR-5884-sensitive reduction in glucose uptake can be taken as an estimate of 3PG flux to serine (Figs. 1 and 5, J_{19}). Since glutamate is a required co-substrate in this pathway, experiments were run in buffer ± glutamine to determine if omission of this amino acid negatively affects serine synthesis by limitation in glutamate availability (see section C for experiments with [1,2-^{13}C] glucose). None of the CBR-5884 treated cell lines exhibited a significant reduction in glucose consumption, either without (Fig. 3A) or with (Fig. 3B) glutamine. Unexpectedly, glucose consumption was higher in CBR-5884-treated LM and BoM lines (with glutamine, p= 0.030 and 0.021 for BoM and LM, respectively; without glutamine p= 0.019 and 0.176, respectively). The increased glucose consumption tended to be higher without glutamine (14.0±2.6% and 11.2±9.6% for BoM and LM, respectively) than with glutamine (3.5±0.9% and 3.8±0.8% for BoM and LM, respectively (Fig. 3C, 3D), which suggests that the absence of exogenous glutamine does not limit serine synthesis. The low number of replicates (n=3) and inherent assay error can account for a lack of statistical significance between the cell lines in the average fraction of glucose used for serine synthesis (one-way ANOVA p= 0.153 without glutamine and 0.567, with glutamine). Given that serine synthesis yields NADH but no lactate, this pathway tends to increase the NADH/NAD ratio, which negatively regulates glycolysis; reduction in this ratio by inhibition of serine synthesis could thus account for the observed increase in glucose uptake (see Discussion).

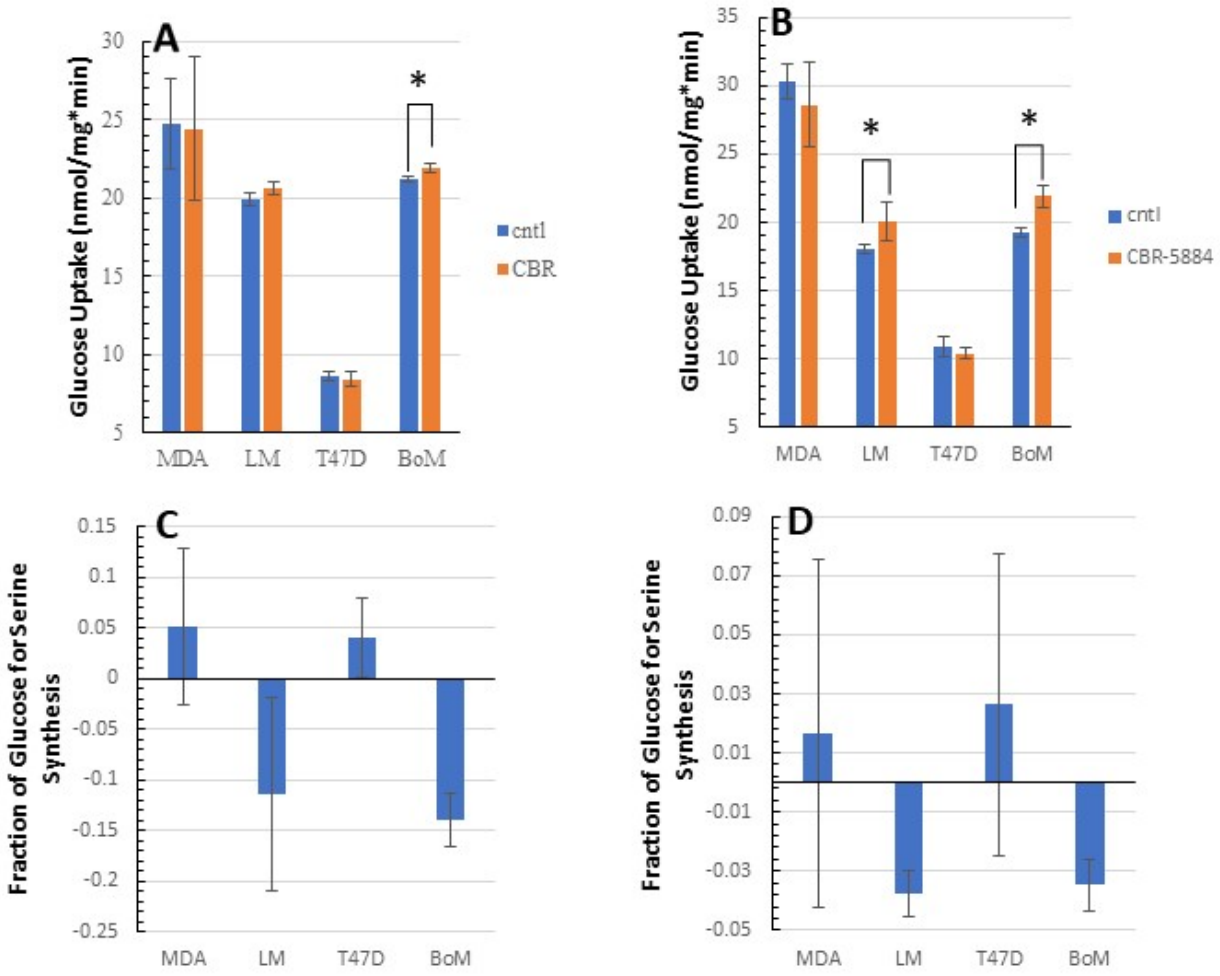

Figure 3: *CBR-5884-sensitive glucose uptake rates for cell lines incubated without (A) or with (B) supplemental glutamine in the media and fractional glucose uptake for serine biosynthesis without (C) or with (D) supplemental glutamine in the media. Cell lines were pre-incubated 2.5 h with 40 µM CBR-5884. The buffer glucose concentrations were determined by enzymatic assay and the rates of uptake were averaged over two 60 min incubation periods. The rates were then normalized to total SDS-soluble protein. The data is presented as the mean ± standard error of the mean (n =3). Flux data in (A) and (B) were analyzed by one-tailed T-test and fractional uptake in (C) and (D) by 1-way ANOVA. Asterisks indicate a significant effect of CBR-5884 treatment.*

C. ^{13}C Enrichment in Serine and Lactate from [1,2-^{13}C] glucose

To further evaluate serine biosynthesis, cells were given [1,2-^{13}C] glucose and the serine exported to the buffer was analyzed by liquid chromatography, triple quadrupole mass spectrometry (LC-TQ MS; Table 2). ^{13}C abundance in serine from MDA-231 cells was no different from background ^{13}C, as measured with unlabeled serine standards (fractional labeling of standards: M=0.9517±0.0038, M1=0.0406±0.0033, M2=0.0076±0.0005, M3=0.0001±0.0001; n=5). In contrast, T47D, BoM, and LM cells showed

significant ^{13}C enrichment above background, indicative of serine biosynthesis in these lines (Table 2). Additionally, the M2 and M3 labeling patterns of LM and BoM cells were significantly greater than that in T47D cells, while the M1 content tended to be greater cells (p=0.059 T47D vs. BoM, p=0.153 T47D vs. LM). These data suggest that the contribution of serine synthesis to labeling the intracellular serine pool and/or the activities of other pathways that rearrange the carbon atoms in serine may differ between these cell lines. From this analysis, the serine efflux rate (Fig. 5, J_{22}) was calculated assuming that accumulation of this amino acid in the buffer over the 60 min incubation periods did not affect the rate of its export (Fig. 4). The LM and BoM cells tended to export serine at a lower rate than T47D cells (Fig. 4; p=0.048 LM vs. T47D; p=0.280 BoM vs. T47D). While these data provide convincing evidence for serine biosynthesis in T47D, LM, and BoM cells, quantitation of 3PG flux to serine (J_{19}) requires additional information on the relative activities of other pathways involved in either consuming serine and/or rearranging the carbon atoms in serine. Glycolysis metabolizes 3PG to pyruvate, which is subsequently reduced to lactate that is exported from the cell. ^{13}C lactate labeling can thus provide needed insight on 3PG labeling, and hence on the potential activities of pathways that rearrange the carbon atoms in serine. ^{13}C lactate enrichment was determined by LC-TQ MS (Table 2) to infer ^{13}C-labeling of 3PG, the glycolytic intermediate that is substrate for serine synthesis. The 3PG carbons are not rearranged in the 3-step serine synthesis pathway, so in principle the labeling pattern in 3PG should be no different from that of serine. In order to infer 3PG labeling, a computational model was used to reproduce the lactate labeling pattern by optimizing 3 flux ratios (Table 3) that have a major impact on ^{13}C labeling in lactate for cells metabolizing [1,2-^{13}C]glucose because of the carbon atom rearrangements that occur in these pathways (Fig. 6): the contribution of the pentose cycle to labeling the hexose phosphate pool ($J_{3af}/(J_0+J_{3af})$, the contribution of malic enzyme to labeling the pyruvate pool ($J_7/(J_{2c}+J_7)$ and the contribution of the forward and reverse non-oxidative pentose phosphate pathway fluxes (J_{3af} and J_{3ar}, respectively) to labeling the ribose phosphate pool (J_{3af}/J_{3ar}). The development of this model has been described in detail elsewhere (22, 23). The model was reasonably effective at reproducing the measured lactate labeling patterns for each cell line, as the errors between the measured and predicted labeling were

small (Tables 2 and 3). From this, the estimated 3PG labeling (Table 4) differed substantially from the serine labeling (Table 2) by having lower M and M1 contents and a higher M2 content. This suggests that, once synthesized, serine is subjected to a cyclic pathway that results in carbon rearrangements in the serine passing through the cycle.

The folate cycle is the most obvious metabolic pathway that can account for carbon rearrangements in serine (Figs. 5 and 6). Since 3PG labeling was similar among the cell lines, but serine labeling differed significantly, this suggests flux through the folate cycle and/or serine synthesis pathway differs between the T47D, BoM, and LM lines. To quantitate these fluxes, a simplified model of the folate cycle was developed to solve for three flux ratios associated with serine synthesis and the cycle that affect ^{13}C enrichment in the serine pool (Fig. 5). Note that because MDA-231 cells did not synthesize serine from glucose, it was not possible to analyze the folate cycle in this cell line. The inputs to the model were the ^{13}C labeling patterns in 3PG and serine, and the background ^{13}C labeling of endogenous serine and glycine, as determined using unlabeled standards.

Table 2: ^{13}C Lactate and Serine enrichment from [1,2 ^{13}C] glucose

Cell Line	Lactate M	Lactate M1	Lactate M2	Lactate M3	Serine M	Serine M1	Serine M2	Serine M3
LM	0.4908 ± 0.0005^{a}	0.0303 ± 0.0005^{a}	0.4660 ± 0.0012$^{a\ b}$	0.0129 ± 0.0005^{a}	0.6658 ± 0.0269$^{b\ d}$	0.1936 ± 0.0148^{a}	0.1343 ± 0.0116^{b}	0.0064 ± 0.0007^{b}
T47D	0.5002 ± 0.0013^{b}	0.0320 ± 0.0006^{a}	0.4589 ± 0.0019^{a}	0.0089 ± 0.0004^{b}	0.8221 ± 0.0064^{a}	0.1416 ± 0.0050^{a}	0.0346 ± 0.0019^{a}	0.0017 ± 0.0002^{a}
BoM	0.4902 ± 0.0018^{a}	0.0328 ± 0.0015^{a}	0.4661 ± 0.0035$^{a\ b}$	0.0109 ± 0.005^{c}	0.6793 ± 0.0473^{b}	0.2053 ± 0.0291^{a}	0.1104 ± 0.0174^{b}	0.0049 ± 0.0008^{b}
MDA	0.4930 ± 0.0020^{a}	0.0251 ± 0.0007^{b}	0.4749 ± 0.0020^{b}	0.0069 ± 0.0006^{d}	0.9525 ± 0.0037^{c}	0.0388 ± 0.0029^{b}	0.0084 ± 0.0007^{a}	0.0003 ± 0.0004^{a}

Unlabeled (M), single (M1), double (M2), and triple (M3) ^{13}C labeled lactate and serine resulting from metabolism of 1,2 ^{13}C glucose was measured in the spent buffer by mass spectrometry. Standards were run in parallel to quantitate the metabolites and the data expressed as fractional content of each label. Data are the mean ± the standard error of six experiments. Differences between cell lines in the fractional content of each labeled species was determined by 1-way ANOVA with Tukey's post-hoc test. Means sharing common superscripts within a column do not significantly differ.

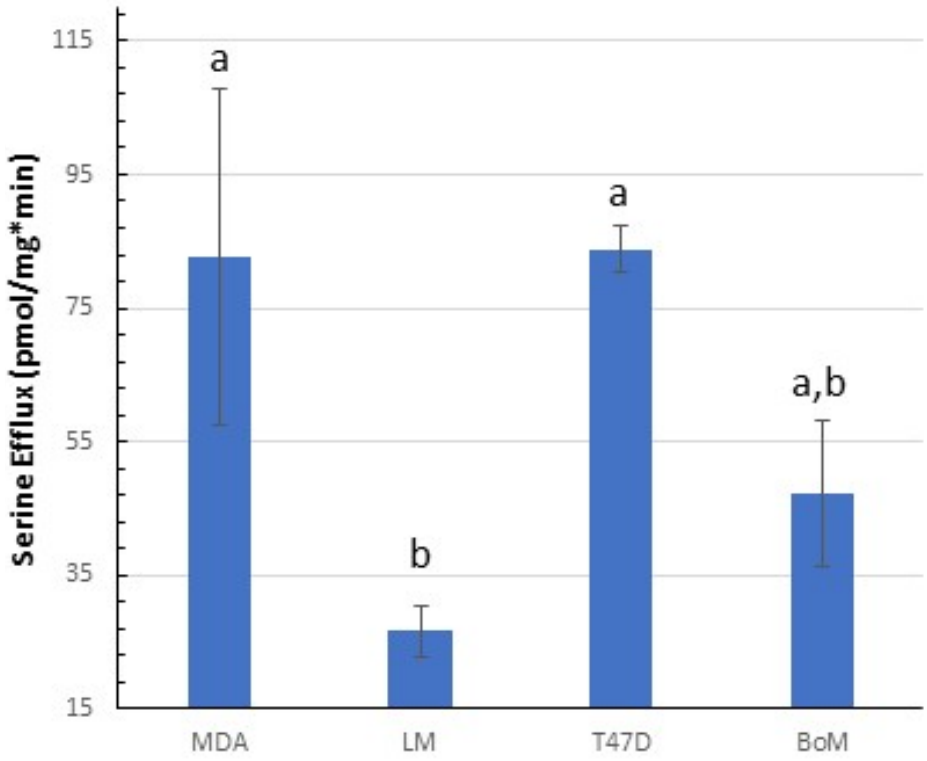

Figure 4: *Serine efflux rates for each cell line measured by LC-TQ mass spectrometry over each 1 h incubation. Data are mean ± standard error of the mean of six experiments. These rates reflect J_{22} in the metabolic maps shown in Figs 5 and 6. Data were analyzed by 1-way ANOVA and Tukey's post-hoc test. Means sharing the same letter are not significantly different.*

Table 3: Model-predicted ^{13}C Lactate Labeling with Model Error and Flux Ratios that were optimized

Cell Line	Lactate M	Lactate M1	Lactate M2	Lactate M3	Model Error	J3af/J3ar	J3af/(J3af+J0)	J7/(J7+J2b)
LM	0.4945 ± 0.0014	0.0305 ± 0.0016	0.4660 ± 0.0012	0.0090 ± 0.0008	0.0100 ± 0.0025	0.2796 ± 0.0376[a]	0.0630 ± 0.0020[c]	0.0501 ± 0.0052[a b]
T47D	0.5020 ± 0.0009	0.0322 ± 0.0016	0.4589 ± 0.0019	0.0069 ± 0.0006	0.0064 ± 0.0031	0.6494 ± 0.0602[a]	0.0899 ± 0.0040[a]	0.0365 ± 0.0034[a]
BoM	0.4918 ± 0.0007	0.0319 ± 0.0027	0.4661 ± 0.0035	0.0102 ± 0.0007	0.0047 ± 0.0030	0.3812 ± 0.1935[a]	0.0540 ± 0.0072[c]	0.0597 ± 0.0050[b]
MDA	0.4930 ± 0.0020	0.0235 ± 0.0008	0.4749 ± 0.0020	0.0085 ± 0.0004	0.0033 ± 0.0006	0.3605 ± 0.0609[a]	0.0316 ± 0.0038[b]	0.0504 ± 0.0029[a b]

Unlabeled (M), single (M1), double (M2), and triple (M3) ^{13}C labeled lactate predicted by the computational model. Computational modeling was used to reproduce the labeling pattern of ^{13}C in lactate within the constraints of the measured fluxes glucose consumption, lactate production, mitochondrial respiration rate. Data are the mean ± the standard error of the mean from six experiments for each cell line. This table can be used to compare the predicted lactate labeling to the measured lactate labeling (Table 2) as well as to analyze the fluxes that were optimized to predict the labeling. The model error is the sum of the absolute values of the difference between the M-M3 predicted and measured labeling Flux ratios were analyzed by 1-way ANOVA with Tukey's post-hoc test. For the optimized flux ratios, means sharing a common superscript are not significantly different.

Table 4: Model-predicted 3-Phosphoglycerate ^{13}C enrichment from 1,2 ^{13}C glucose

Cell Line	M	M1	M2	M3
LM	0.5102 ± 0.0005	0.0151 ± 0.0005	0.4739 ± 0.0009	0.0008 ± 0.00004
T47D	0.5133 ± 0.0007	0.0208 ± 0.0009	0.4647 ± 0.0017	0.0011 ± 0.0001
BoM	0.5105 ± 0.0014	0.0132 ± 0.0015	0.4759 ± 0.0030	0.0004 ± 0.0002
MDA	0.5087 ± 0.0015	0.0078 ± 0.0007	0.4835 ± 0.0022	<0.0001 ± <0.0001

Unlabeled (M), single (M1), double (M2), and triple (M3) ^{13}C labeled 3-Phosphoglycerate predicted by the computational model whose optimized flux ratios are shown in Table 3. Data are the mean ± the standard error of the mean for each cell line.

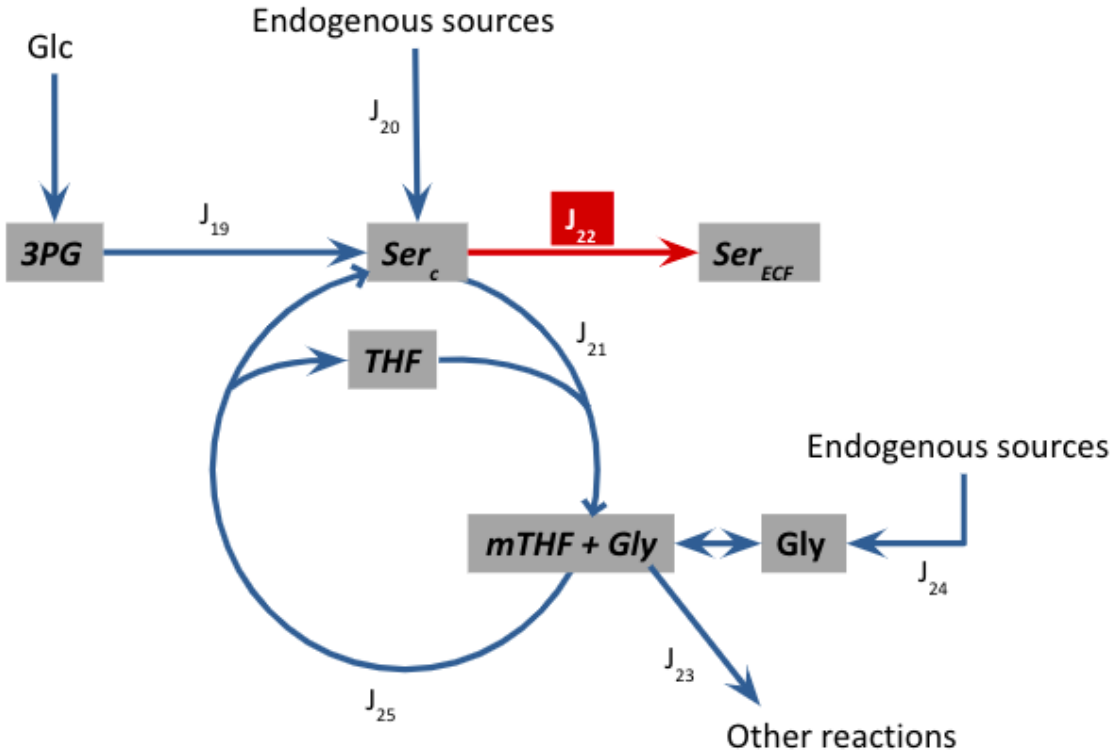

Figure 5: *A simplified model of the folate cycle. Serine efflux and extracellular ^{13}C serine labeling were measured by LC-TQ MS. 3PG ^{13}C labeling was inferred from modeling ^{13}C lactate labeling. Serine consumption was assumed to occur through two processes- serine export from the cell and de-methylation to glycine, which in turn is used by various reactions, including glutathione synthesis. Endogenous sources of serine and glycine were assumed to be from protein turnover. Abbreviations: 3PG: 3-phosphoglycerate, Ser_c: cytoplasmic serine, Ser_{ECF}: extracellular serine, THF: tetrahydrofolate, mTHF: methyl-tetrahydrofolate, Gly: cytoplasmic glycine. Flux notations: J_{19}: serine synthesis from 3PG, J_{20}: serine from protein turnover*

contributing to cytoplasmic serine pool, J_{21}: de-methylation of serine in the folate cycle by serine hydroxyl-methyltransferase, J_{22}: serine export to the extracellular fluid, J_{23}: cellular glycine consumption, J_{24}: glycine from protein turnover contributing to the cytoplasmic glycine pool, J_{25}: methylation of glycine to serine in the folate cycle.

From the model, the optimized flux ratios affecting serine labeling are the contribution of serine synthesis to the cytoplasmic serine ($J_{19}/(J_{19}+J_{20})$), the contribution of the folate cycle to labeling of the cytoplasmic glycine pool ($J_{21}/(J_{21}+J_{24})$), and the fraction of serine that recycles through the folate cycle ($J_{25}/(J_{19}+J_{20})$). The great majority of the 3PG was either unlabeled or double-labeled (Table 4), with the latter labels largely occurring at carbons 2 and 3. The recycling of unlabeled and 2,3 labeled serine through the folate cycle will result in enrichment of M1 serine at the expense of M2 serine as carbon 3 is transferred to tetrahydrofolate (Fig. 6). The model was effective in reproducing the serine labeling pattern, as demonstrated by the extremely low errors (Table 5; and compare serine labeling with Table 2). It is notable that the T47D line differed from the BoM and LM lines, which is not surprising given that the M1 and M2 serine labeling in the T47D line tended to be lower than the BoM and LM lines. The contribution of serine synthesis to labeling the serine pool was higher in the more malignant LM and BoM lines, while the fraction of serine recycling through the folate cycle was significantly lower in these lines compared to T47D cells (Table 5).

Table 5: Folate cycle model results

Cell Line	M	M1	M2	M3	J19/(J19+J20)	J21/(J21+J24)	J25/(J19+J20)	Model Error
LM	0.6660 ± 0.0270	0.1936 ± 0.0148	0.1343 ± 0.0116	0.0061 ± 0.0008	0.6403 ± 0.1043[a b]	0.3658 ± 0.2008[a]	0.0561 ± 0.0015[b]	0.0001 ± 0.0001
T47D	0.8221 ± 0.0065	0.1416 ± 0.0050	0.0346 ± 0.0019	0.0017 ± 0.0002	0.2993 ± 0.0292[a]	0.1392 ± 0.1006[a]	0.1095 ± 0.0033[a]	<0.0001 ± <0.0001
BoM	0.6793 ± 0.0473	0.2051 ± 0.0289	0.1103 ± 0.0173	0.0053 ± 0.0012	0.6904 ± 0.1455[b]	0.1982 ± 0.1606[a]	0.0658 ± 0.0032[b]	0.0001 ± 0.0008

Unlabeled (M), single (M1), double (M2), and triple (M3) ^{13}C labeled serine predicted by the computational folate cycle model depicted in Fig. 5. Computational modeling was used to reproduce the labeling pattern of ^{13}C in serine by optimizing three flux ratios: $J_{19}/(J_{19}+J_{20})$, $J_{21}/(J_{21}+J_{24})$, and $J_{25}/(J_{19}+J_{20})$. Data are the mean ± the standard error of the mean of six experiments for each cell line. The model error is the sum of the absolute values of the difference between the M-M3 predicted and measured labeling. Flux ratios were analyzed by 1-way ANOVA with Tukey's post-hoc test. Within a column, means sharing common superscripts are not significantly different.

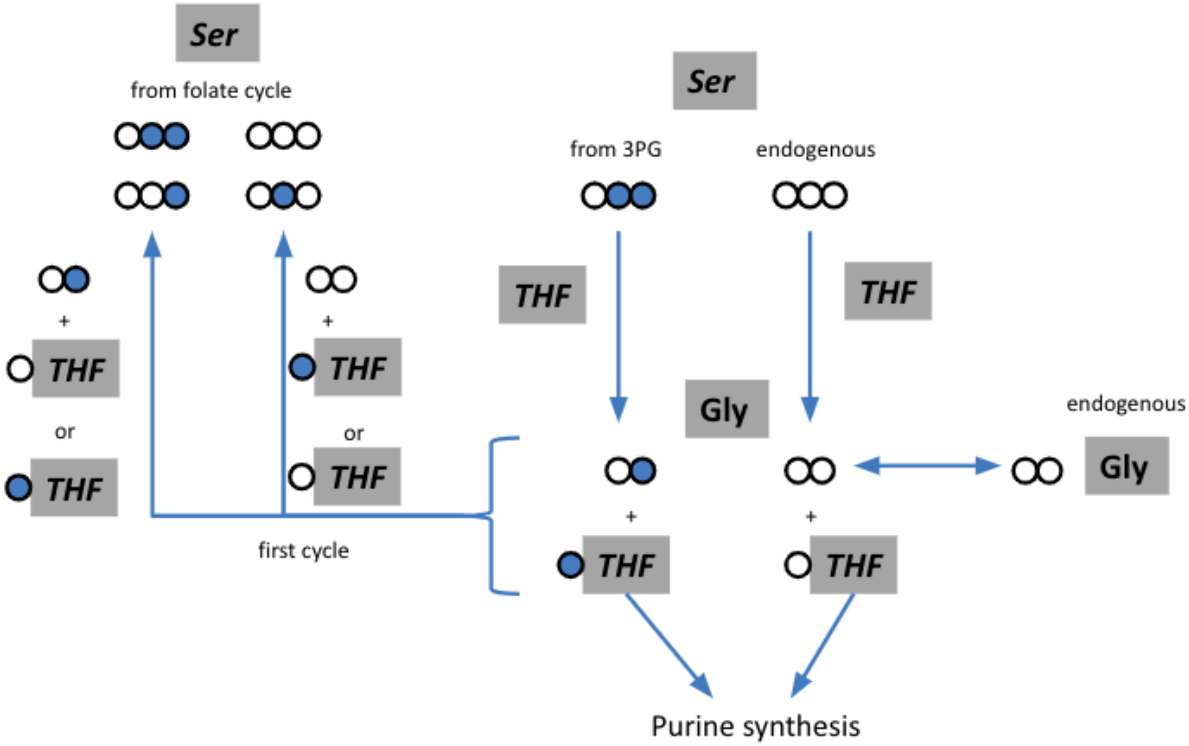

Figure 6: *Carbon atom transitions within the folate cycle to predict its impact on serine labeling. Unlabeled carbon atoms are depicted as open circles and ^{13}C carbons as filled circles. Carbons in serine (Ser) and glycine (Gly) are numbered from left to right. About half of the serine from biosynthesis is double-labeled at positions 2 and 3, while the other half and approximately 96% of endogenous serine is unlabeled. As serine enters the folate cycle, carbon 3 is transferred to tetrahydrofolate (THF). The methyl group can be used for purine synthesis, in which case the resulting glycine affects the labeling of the cytoplasmic glycine pool. Alternatively, the methyl group can be transferred to glycine; the probability of ^{13}C transfer to unlabeled glycine to form M1 serine is much greater than transfer to M1 glycine to form M2 serine because of the high proportion on unlabeled glycine. This enriches M1 serine and depletes M2 serine. The steady-state fractional labeling in serine was determined from twenty rounds of this cycle.*

E. Calculating Pathway Fluxes

Determination of folate cycle fluxes required knowing at least two of the seven fluxes in addition to the flux ratios determined by the folate cycle model. Along with serine efflux (J_{22}), a minimal estimate of glycine consumption (J_{23}) can be assessed from the BSO-sensitive glutamine consumption seen for T47D and BoM lines since glycine is also required for GSH synthesis (see Methods for a detailed explanation). This approach was not possible for LM cells since they lacked BSO-sensitive glutamine uptake, but a minimal estimate of J_{19} was obtained from the ^{13}C model employed to reproduce lactate labeling from [1,2-^{13}C] glucose. Without serine synthesis, the model was inadequate for LM cells because malic enzyme

flux, which enriches M1 and M3 pyruvate, was limited by a combination of insufficient NADH from glycolysis and low mitochondrial respiration rate. Pyruvate produced by malic enzyme does not generate NADH, so another source of this reducing equivalent such as the serine synthesis pathway is required. Inclusion of a serine synthesis flux established by the model significantly reduced the error between the calculated and measured ^{13}C lactate enrichment. This insight justifies quantitation of J_{19} in this way, and suggests that serine synthesis is an important controller of malic enzyme activity.

Serine synthesis flux in T47D cells was minimal, consuming only 0.13±0.02% of glucose. Approximately 22% of the serine supplied by J_{19} and J_{20} entered the folate cycle (J_{21}) while 78% was exported; 1.6% of the serine entering the cycle returned to the serine pool (J_{25}) and the rest was consumed for GSH synthesis. Serine metabolism in T47D cells has been previously investigated by Dolfi et al (24). From their results (personal communication with A. Vazquez), we calculated that T47D serine consumption for purposes other than protein synthesis was 3.42% of glucose consumption (consumption for protein synthesis was excluded since exogenous essential amino acids were not present in our experiments). Folate cycle fluxes calculated from this result were very similar to those based on BSO-sensitive glutamine consumption (J_{19}= 31±3, J_{21} = 44±33, J_{23} = 305 ± 26, and J_{25} = 13 ± 4 pmol/min x mg; compare to Table 6).

With the exception of serine export, fluxes in LM cells were more than an order of magnitude greater than T47D cells. Serine synthesis accounted for 1.3% of glucose consumption. Remarkably, 96.7% of serine supplied by J_{19} and J_{20} entered the folate cycle, with only 3.3% exported. Similar to T47D cells, only 2.0% of the serine entering the cycle was recycled to the serine pool. The results indicate that the more malignant LM cell line has a higher demand for serine, possibly to support greater demand for nucleotide synthesis in these rapidly proliferating cells, and this corresponds with a lower rate of serine efflux.

BoM cells were similar to the LM line in serine labeling pattern (Table 2), folate cycle model-optimized flux ratios (Table 5), glucose consumption (Fig 8), and increase in glucose consumption with CBR-5884 (Fig. 3). In this respect, it was surprising that the fluxes determined using BSO-sensitive glutamine consumption were more similar to T47D cells (Table 6, BoM[a]). Serine synthesis consumed only 0.11% of

glucose and 43% of serine supplied by J_{19} and J_{20} entered the folate cycle. It is likely that the BSO-sensitive glutamine uptake substantially underestimates glycine consumption (J_{23}). To test this, an alternative approach was taken in which J_{19} was determined from the fractional M2 serine content and glucose consumption using the significant linear regression observed between M2 serine and ratio J_{19}/J_0 for LM and T47D cells (Fig. 7). The fact that data from both cell lines form a single regression line with a high correlation coefficient suggests that the relationship between M2 serine and J_{19}/J_0 is not unique for each cell type and can be applied to BoM cells. From this analysis, J_{19} was about 80% of that seen in LM cells, and 0.96% of glucose was used for serine synthesis (Table 6, BoM[b]). Approximately 92% of serine from J_{19} and J_{20} entered the folate cycle, with 1.3% recycling.

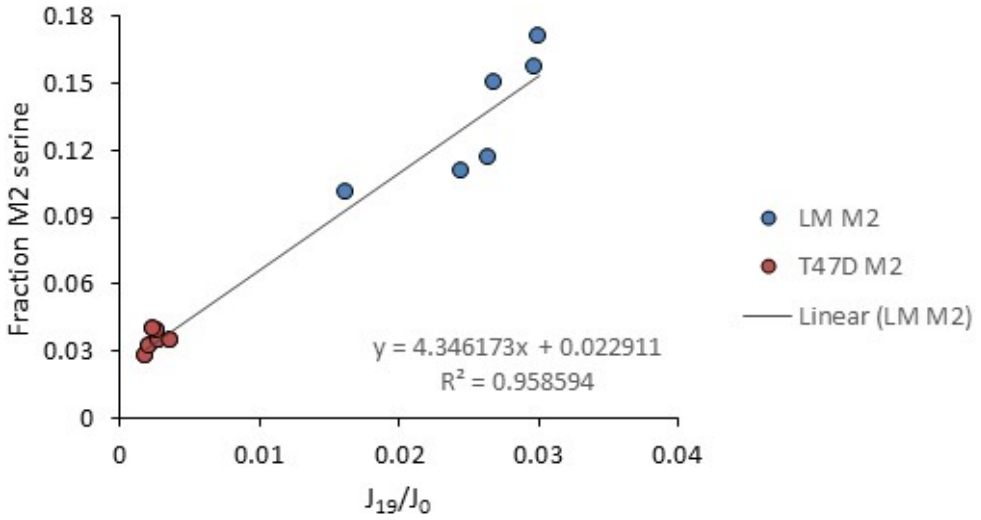

Figure 7: *Dependence of M2 serine on the ratio of flux through the serine synthesis pathway (J_{19}) to glucose uptake (J_0). Data from LM and T47D cells were combined and the least-squares regression equation used to calculate J_{19}/J_0 for each experiment with BoM cells.*

Table 6: Calculated Fluxes within the Folate Cycle

Cell Line	J19	J20	J21	J23	J24	J25
LM	477 ± 54[b]	319 ± 115[a]	814 ± 89[a]	12131 ± 4605[b]	11361 ± 4660[a]	44 ± 4[a]
T47D	29 ± 3[a]	79 ± 22[a]	37 ± 27[a]	248 ± 19[a]	223 ± 32[a]	12 ± 3[a]
BoM[a]	43 ± 11[a]	40 ± 32[a]	41 ± 34[a]	169 ± 10[a]	133 ± 28[a]	5 ± 1[b]
BoM[b]	373 ± 70	197 ± 97	559 ± 47	14526 ± 3879	14004 ± 3910	37 ± 3

Fluxes are expressed as pmol substrate consumed per minute per mg cell protein. For T47D and BoM[a], folate cycle fluxes J_{19}, J_{20}, J_{21}, J_{24}, and J_{25} were calculated from the optimized flux ratios (Table 5), J_{22} (Fig. 4), and an estimate of J_{23} from BSO-sensitive glutamine uptake (see Methods for details). BoM[b] fluxes were based on an estimate of J_{19} from the Fig. 7 regression plot. For LM cells, the fluxes J_{20}, J_{21}, J_{23}, J_{24}, and J_{25} were calculated from the optimized flux ratios (Table 5), J_{22} (Fig. 4), and an estimate of J_{19} from the computational model used to reproduce the ^{13}C lactate labeling pattern. Data are the mean ± the standard error of the mean of six experiments for each cell line. Fluxes for LM, T47D, and BoM[a] were analyzed by 1-way ANOVA and Tukey's post-hoc test. Within a column, means sharing common superscripts are not significantly different. Flux notations: J_{19}: serine synthesis from 3PG, J_{20}: serine from protein turnover contributing to cytoplasmic serine pool, J_{21}: de-methylation of serine in the folate cycle by serine hydroxyl-methyltransferase, J_{22}: serine export to the extracellular fluid, J_{23}: cellular glycine consumption, J_{24}: glycine from protein turnover contributing to the cytoplasmic glycine pool, J_{25}: methylation of glycine to serine in the folate cycle.

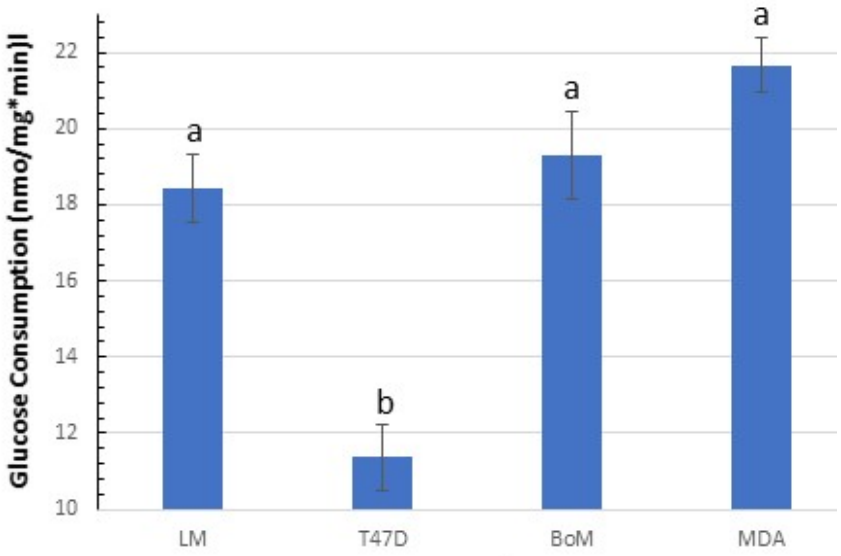

Figure 8: *Glucose consumption rates for each cell line measured by metabolite assay. Data are mean ± standard error of the mean of six experiments. These rates reflect J_0 in the metabolic maps shown in Fig. 1 of the introduction. Data were analyzed by 1-way ANOVA and Tukey's post-hoc test. Means sharing the same letter are not significantly different.*

Discussion

The overall goal of this research was to determine if metastatic sub-clones, both derived from the TNBC metastatic MDA-MB-231 breast cancer cell line, that preferentially invade and grow in lung or bone tissue exhibit metabolic differences in serine and glutathione biosynthesis. Metabolic plasticity is potentially important for secondary tumor growth in different tissue microenvironments, and may guide development of metastatic tumor-specific, metabolic-targeted therapies. Therefore, fluxes through these anabolic pathways were quantified using the principles of ^{13}C metabolic flux analysis with ^{13}C glutamine and ^{13}C glucose as substrates. The major findings from this study were that (a) none of the exogenous glutamine consumed by LM cells was used for GSH synthesis compared to approximately 10% used by MDA-231, T47D, and BoM lines, (b) LM and BoM lines exhibited relatively high rates of serine synthesis, while the parent MDA-231 line had no detectable flux through this pathway, and (c) LM and BoM lines exhibited greater folate cycle fluxes than the less malignant T47D line.

Glutathione is a tripeptide of glutamate, cysteine, and glycine; hence, glutamine consumption through its conversion to glutamate, and serine consumption through the folate cycle to glycine, are indirect substrates in the production of GSH. GSH becomes oxidized to glutathione disulfide (GSSG) during periods of oxidative stress, and the GSH:GSSG ratio is thus an indicator of oxidative stress (25). GSH combats oxidative stress by acting as an essential cofactor for a class of enzymes called glutathione peroxidases (Gpxs) where it serves as a source of electrons to reduce hydrogen peroxide and lipid peroxides to less reactive forms (17, 26). Glutaredoxins (Grx), members of the thioreductase superfamily, are GSH-dependent oxidoreductase enzymes that catalyze the thiol-disulfide exchange, primarily from GSH to protein thiols or protein disulfides (19, 27). The conversion of GSSG back to its reduced form, GSH, is catalyzed by Grxs and glutathione reductases through the oxidation of NADPH, a product of the

oxidative pentose phosphate pathway and malic enzyme (17). Grxs' primary importance is to protect protein thiols, the main target of ROS species, from oxidation by adding GSH to the thiol through a process called glutathionylation, preventing irreversible oxidation (28).

Elevated GSH levels are observed in many types of tumors, and they commonly make such tumors more resistant to treatment as they prevent oxidative stress triggered by radiation and chemotherapies (29). GSH primarily acts as a cytoprotector by preventing damage to proteins or DNA that may induce apoptosis, but also by detoxifying other dangerous chemicals within the cell, especially chemotherapeutics, allowing GSH to potentially serve as a marker for increased higher risk of metastasis (30). One study found that TNBC cells maintained and enhanced Gpx1 expression as opposed to non-TNBC cell lines; Gpx1 protected focal adhesion kinase (FAK) from oxidation (20). FAK is responsible for the critical step of metastasis by creating high affinity binding sites in secondary tissues during metastasis, and when it is oxidized, the pathway becomes dysregulated, leading to a reduced proliferation of TNBC cells to the lungs (20). This makes the synthesis of glutathione an attractive target for some types of metastatic cancers.

The current study suggests that MDA-231, T47D, and BoM cells use approximately 10% of exogenous glutamine for GSH synthesis. Notably, the more metastatic MDA-231 and BoM lines did not exhibit higher glutamine demand for GSH than the less aggressive T47D line. This does not exclude the possibility that MDA-231 and BoM cells synthesize GSH at a higher rate, as these results do not account for use of endogenous glutamate in GSH synthesis. Much of the remaining 90% of glutamine consumption is for fatty acid synthesis, ATP production through the TCA cycle, and as a source of carbons for reactions such as the malic enzyme pathway which consume TCA metabolites (16). The LM cell line had no detected glutamine consumption for GSH synthesis, which does not support our hypothesis that lung-specific tumors have a higher demand for antioxidants such as GSH. The lungs having a higher oxygen partial pressure (approximately 100 mmHg) than the systemic tissues (where it can range from 20-40 mmHg), which is predicted to increase the probability of superoxide production by the mitochondrial respiratory chain (and correspondingly the production of ROS derived from

superoxide) in this higher oxygen environment. It is possible that LM cells have sufficient internal glutamate and/or glutamine stores to support high rates of GSH synthesis and so do not require exogenous glutamine. Alternatively, these cells may have adopted other metabolic features for growth in the lungs; they could rely predominantly on peroxyredoxins and thioredoxins, which do not require GSH, for defense against ROS, and/or on substrate limitation to mitochondria, which would limit superoxide production. The latter possibility is supported by experiments (data not shown) showing that mitochondrial respiration rate of LM cells is significantly less than the other three cell lines.

Serine metabolism is frequently dysregulated in cancers as it serves as a converging point for biosynthesis of metabolites that are necessary to fuel the proliferative state of cancers (31). During the biosynthesis of serine from 3PG, 2-oxoglutarate is formed from glutamate, which can be used to supply carbons to the TCA cycle. Serine is a direct precursor to both glycine and cysteine through the transsulfuration pathways, and glycine is directly used in nucleotide base synthesis and glutathione synthesis (31). Serine is a major donor of 1-Carbon units to the folate and methionine cycles as well as the transsulfuration pathway. In the folate cycle, serine is converted to glycine by serine hydroxymethyltransferase-2 (SHMT-2). The carbon 3 methyl group is transferred to tetrahydrofolate (THF) to form methyl-tetrahydrofolate (mTHF) (Fig. 6). mTHF links the folate cycle to the methionine cycle by donating its methyl group to homocysteine, producing cysteine, a constituent of GSH (33). The folate cycle also helps to maintain cellular ATP and GTP levels through de novo purine synthesis (14). Serine is also required for the synthesis of sphingolipids and phosphatidylserine, and the demand for lipids to build lipid membranes of growing cells are elevated in cancers (31). Cancers with a higher capacity for serine synthesis and flux into the folate cycle (Fig. 5, J_{21}) are thus less reliant on the potentially limited availability of extracellular serine for regulation of redox homeostasis, production of nucleotides, and synthesis of lipids and proteins. Indeed, recent studies have shown that MDA-231 cells have a low capacity for serine synthesis as their growth is completely inhibited in the absence of exogenous serine (32).

Metabolic profiling in MDA-MB-231 and its tissue-specific subclones to brain (BrM) and bone (BoM) have revealed a dependency on serine and the 1-carbon cycles to drive proliferation (34). SHMT-2

expression is upregulated in BrM and BoM tissue-specific subclones in comparison to the primary breast tumor, and inhibition of the rate-limiting step catalyzed by SHMT-2 suppresses the proliferation of metastatic subclones (34). This suggests SHMT-2 activity and upregulation play a direct role in the ability of cells in the primary breast tumor to adapt their metabolic phenotype to proliferate and colonize a secondary tissue. In the more proliferative BrM and BoM cell lines, Li et al 2020 observed an increase in the glycolytic intermediate, dihydroxyacetone-phosphate (DHAP; which can be isomerized the glyceraldehyde-3-phosphate, the precursor of 3PG) as well as a significant decrease in free nucleotides in comparison to the maternal cell line. . The reduction of free nucleotides is attributed to the elevated demand of nucleotides for the BoM and BrM cell lines which have higher proliferation rates. Taken together with evidence that inhibition of PHGDH does not affect growth of primary breast tumors but does inhibit BrM growth, and that elevated PHGDH expression is necessary for proliferation in serine-depleted environments, glucose conversion to serine becomes the primary pathway supporting SHMT-2 activity and the folate cycle (39). Thus, in subclonal, metastatic cell lines, it is a dependency on de-novo serine biosynthesis through PHGDH overexpression, as opposed to use of exogenous serine pools in parental cells, that fuels serine catabolism pathways that could be important for growth in secondary tissue microenvironments (39).

PHGDH expression and ^{13}C enrichment in serine from glucose in the MDA-MB-231 cell line are low compared to many cancers, showing this cell line has little to no de novo serine biosynthesis (35, 36). Furthermore, without exogenous serine in the media, proliferation of MDA-231 cells is significantly inhibited, whereas other cell lines with a high capacity for serine synthesis are unaffected (21, 34). The present results confirm these findings, as there was no detectable ^{13}C labeling of serine in the MDA-231 cells above background ^{13}C (Table 2). The enhanced de novo serine biosynthesis in LM and BoM cells, indicates that extracellular serine availability is not a limitation to growth in their respective microenvironments. Given that LM and BoM have higher proliferation rates compared to the MDA-231 parent line, this metabolic change is likely advantageous for the cell lines to adopt a more aggressive phenotype. While BoM cells did not synthesize serine at a higher rate than the LM line as originally

hypothesized, this pathway may be particularly important for BoM cells, as extracellular serine availability may be particularly limiting given that mass-adjusted blood flow to bone is approximately 150-250-fold lower than that to the lungs (37). Additionally, serine stimulates the production of osteoclasts, which mediate bone demineralization and degradation (38). Serine produced in excess of that needed for proliferation and exported from cells could thus contribute to bone destruction.

Serine synthesis was also detected in T47D cells, but the pattern of ^{13}C enrichment differed from LM and BoM lines, suggesting the rates of synthesis and/or the recycling of serine through the folate cycle differ (Table 2). In support of this, the BoM and LM cells exhibited similar increases in glucose consumption when serine synthesis was inhibited with CBR-5884, but the T47D cells did not (Fig 3). While a decrease in glucose consumption was expected, the results are consistent with the possibility that NADH production by the serine pathway is sufficiently robust in LM and BoM lines to inhibit glycolysis by increasing the cytoplasmic NADH:NAD ratio, which is an allosteric regulator of glycolysis. Glycolytic production of NADH leads to stoichiometric production of pyruvate, which can subsequently be reduced to lactate by the NADH-dependent lactate dehydrogenase; thus, when a high proportion of pyruvate is reduced to lactate, as in most cancers, this flux tends to lower the NADH:NAD ratio. With the serine synthesis pathway active, NADH is produced but pyruvate is not, so the resulting NADH may not be required by lactate dehydrogenase, thereby potentially increasing the NADH:NAD ratio. Relieving such allosteric inhibition with CBR-5884 could more than offset the reduction in glucose uptake due to loss of 3PG conversion to serine. Alternatively, it is possible that 3PG flux to serine does not differ between these three lines, but that LM and BoM glycolytic enzymes are more sensitive to allosteric inhibition by NADH than the same enzymes in T47D cells. However, the differences in ^{13}C serine enrichment between these lines (particularly M2 content; see Fig. 7) suggests the 3PG to serine fluxes differ and that such a difference impacts NADH:NAD and allosteric regulation of glycolysis. This is further supported by the folate cycle predicted contribution of serine synthesis to labeling the cytoplasmic serine pool (J_{19} /(J_{19}+ J_{20}); Table 5). Serine synthesis accounted for approximately 30% of the serine production in T47D cells

compared to 64-69% for LM and BoM cells. Taken together, these data indicate a more active serine synthesis pathway in LM and BoM cells than T47D cells.

The flux of 3PG to serine and all folate cycle fluxes for T47D and BoM cells were determined from the measured ^{13}C serine labeling pattern, the model-inferred 3PG ^{13}C labeling pattern, the model-inferred folate cycle flux ratios, the serine efflux rate (J_{22}), and the BSO-sensitive glutamine uptake rate, the latter of which is an estimate of glycine consumption for GSH synthesis (J_{23}). The true glycine consumption is likely higher than this since it does not account for other reactions (e.g., glycine export) that use this amino acid; in turn, this may underestimate serine synthesis flux. Only 0.13% of glucose consumed by T47D cells was used to synthesize serine. A detailed study of amino acid uptake rates and protein synthesis rate in T47D cells by Dolfi et al (2013) allowed an alternative estimate of cellular glycine consumption (J_{23}). From their data, we calculated that T47D serine demand was 5.16% of glucose uptake, but 3.42% of glucose uptake without protein synthesis. The latter was used to estimate T47D serine consumption through the folate cycle (i.e., $J_{23}= J_0*0.0342 – J_{22}$) and hence serine synthesis flux in the current experiments since little to no protein synthesis is expected in the absence of essential amino acids. There was good agreement between these approaches (3PG conversion to serine averaged 29±3 and 31±3 pmol/min x mg using BSO-sensitive glutamine uptake and Dolfi et al data, respectively), suggesting that the use of BSO-sensitive glutamine consumption, at least for T47D cells, is a reasonable approximation of J_{23}. However, this analysis yielded a similarly low 3PG to serine flux for BoM cells (43±11 pmol/min x mg; Table 6), despite evidence from the CBR-5884 experiments and ^{13}C serine enrichment implicating a higher flux; thus the BSO-sensitive glutamine consumption is likely a significant underestimate of J_{23}, and hence J_{19}, in BoM cells. As an alternative approach, 3PG to serine flux was calculated from the measured M2 serine content (Table 2) using the significant positive correlation between the fraction of serine M2 and the ratio of serine synthesis to glucose uptake for LM and T47D cells (Fig. 7). By this approach, serine synthesis was an order of magnitude greater than that estimated by BSO-sensitive glutamine uptake (0.92% of glucose converted to serine) and similar to LM cells (1.3% of glucose converted to serine). Serine consumption by the folate cycle was approximately two orders of magnitude

greater than the previous estimate, and suggests glycine efflux is considerably greater than serine efflux. The results are consistent with the CBR-5884 experiments and ^{13}C serine labeling and thus a better approximation of the fluxes.

Glycine demand for GSH synthesis could not be estimated for LM cells since they lacked a BSO-sensitive glutamine consumption. Notably, the model developed to reproduce ^{13}C lactate enrichment from [1,2-^{13}C] glucose was ineffective assuming no 3PG to serine flux, as this constrained malic enzyme flux, which is the pathway most important for enriching M1 and M3 lactate as carbons are shuffled in the TCA cycle. This constraint occurs because the only two pyruvate producers in the model are glycolysis and malic enzyme, and these must balance the rates of pyruvate consumed by lactate dehydrogenase and mitochondria (Fig. 1). Increased malic enzyme flux, by necessity, reduces glycolytic pyruvate and thus NADH supply; however, a minimum rate of NADH supply, set by the measured rate of lactate production, is necessary. Serine synthesis was therefore determined by the model as the flux necessary to supply NADH at a rate sufficient for malic enzyme to minimize the error in reproducing ^{13}C lactate labeling. This indicates that serine biosynthesis is an important source of NADH production for lactate production, as it is required for the reduction of malate-generated pyruvate into lactate. Also, the production of 2-oxoglutarate during biosynthesis of serine may be used a source of carbons to produce malate, which is catalyzed by malic enzyme into pyruvate. The malic enzyme pathway also generates NADPH, the reducing equivalent used by Gpxs alongside GSH to provide antioxidant defense for protein thiols. Because J_{19} was established in this way, it likely underestimates the true flux given that NADH production is expected to be greater than the rate of malic enzyme flux if it is to significantly increase the NADH:NAD ratio to affect glycolysis, as suggested by the CBR-5884 experiments.

Conclusion

In summary, the results do not support the hypothesis that BoM cells have higher rates of serine synthesis than the other cell lines; the higher serine synthesis rates and folate cycle fluxes in both LM and BoM subclones are likely important to support their higher rates of proliferation than the MDA-231 and T47D lines by increasing substrate availability for purine nucleotide synthesis, and/or increasing NADH and α-ketoglutarate synthesis to support the TCA cycle and malic enzyme. The results did not support the hypothesis that LM cells have a higher rate of GSH synthesis and a higher proportion of glutamine used for GSH synthesis to protect against the more oxygen-rich lung microenvironment. This surprising result suggests that LM cells may rely on peroxiredoxins and/or thioredoxins as antioxidant defense mechanisms rather than on glutathione peroxidases and glutaredoxins. Since the T47D cell line is characterized as being less metastatic and slower to proliferate than LM and BoM cell lines, the biosynthetic and metabolic requirements to fuel its proliferation will be less. The reduced glucose consumption seen in T47D cells comparatively as well as the significantly lower flux of 3-phosphoglycerate to serine, confirms the notion that T47D cells require less serine biosynthesis for various biosynthetic reactions within the 1-Carbon cycle that contribute to GSH, fatty acid, NAD(P)H, and amino acid production. Taken together, these differences illustrate there are changes in metabolic phenotype among these metastatic breast cancer subclones. More studies are required to determine if these metabolic changes facilitate metastasis of LM and BoM line to lung or bone, respectively.

References

1. Hirschey, Matthew D. et al. (2015). Dysregulated metabolism contributes to oncogenesis. *Seminars in Cancer Biology,* 35:S129-S150
2. Hiller, Karsten and Metallo, Christian. (2013). Profiling metabolic networks to study cancer metabolism. *Current Opinion in Biotechnology,* 24(1):60-68.
3. DeBerardinis, Ralph. and Chandel, Navdeep. (2016). Fundamentals of cancer metabolism. *Science Advances,* 2(5):e1600200
4. Gentric, Geraldine., Mieulet, Virginie., and Mechta-Grigoriou, Fatima. (2017). Heterogeneity in Cancer Metabolism: New Concepts in an Old Field. *Antioxidants and Redox Signaling,* 26(9):462-485.
5. Jia, Dongya et al. (2019). Elucidating cancer metabolic plasticity by coupling gene regulation with metabolic pathways. *Proceeding of the National Academy of Sciences of the United States of America,* 116(9):3909-3918.
6. Pavlova, Natalya and Thompson, Craig. (2016). The Emerging Hallmarks of Cancer Metabolism. *Cell Metabolism,* 23(1):27-47.
7. Minn, Andy et al. (2005). Distinct organ-specific metastatic potential of individual breast cancer cells and primary tumors. *The Journal Clinical Investigation,* 115(1):44-55.
8. Gupta, G.P. et al. (2005). Identifying Site-specific Metastasis Genes and Functions. *Cold Spring Harbor Symposia on Quantitative Biology,* 70:149-158.
9. Bos, Paula et al. (2009). Genes that mediate breast cancer metastasis to the brain. *Nature,* 459(7249):1005-1009.
10. Minn, Andy et al. (2005). Genes that mediate breast cancer metastasis to lung. *Nature,* 436(7050):518-524.
11. Kang, Yibin et al. (2003). A multigenic program mediating breast cancer metastasis to bone. *Cancer cell,* 3(6):537-549.
12. Abdel-Wahab, Ali., Mahmoud, Waheed., and Al-Harizy, Randa. (2019). Targeting glucose metabolism to suppress cancer progression: prospective of anti-glycolytic cancer therapy. *Pharmacological Research,* 150:104511.
13. Zogg, Cheryl. (2014) Phosphoglycerate Dehydrogenase: Potential Therapeutic Target and Putative Metabolic Oncogene. *Journal of Oncology,* 2014:1-13.
14. Yang, Ming and Vousden, Karen. (2016). Serine and one-carbon metabolism in cancer. *Nature Reviews Cancer,* 16(10):650-662.
15. Cho, Hyun Min., Jun, Do youn., Bae, Myung Ae., Ahn, Jong Deok., and Kim, Young Ho. (2000). Nucleotide sequence and differential expression of the human 3-phosphoglycerate dehydrogenase gene. *Gene,* 245(1):193-201.
16. Daye, Dania and Wellen, Kathryn. (2012). Metabolic reprogramming in cancer: Unraveling the role of glutamine in tumorigenesis. *Seminars in Cell and Developmental Biology,* 23(4):362-369.

17. Traverso, Nicola et al. (2013). Role of Glutathione in Cancer Progression and Chemoresistance. *Oxidative Medicine and Cellular Longevity,* 2013:1-10.
18. Dakubo, G. D. (2006). Altered metabolism and mitochondrial genome in prostate cancer. *Journal of Clinical Pathology,* 59(1):10-16.
19. Lu, J., Chew, E-H., and Holmgren, A. (2007). Targeting thioredoxin reductase is a basis for cancer therapy by arsenic trioxide. *Proceedings of the National Academy of Sciences,* 104(30):12288-12293.
20. Lee, Eunkyung et al. (2020). Glutathione peroxidase-1 regulates adhesion and metastasis of triple-negative breast cancer cells via FAK signaling. *Redox Biology,* 29:101391.
21. Mullarky, Edouard et al. (2016). Identification of a small molecule inhibitor of 3-phosphoglycerate dehydrogenase to target serine biosynthesis in cancers. *Proceedings of the National Academy of Sciences,* 113(7):1778-1783.
22. Gebril, Hoda., Avula, Bharathi., Wang, Yan-Hong., Khan, Ikhlas., and Jekabsons, Mika. (2016). ^{13}C Metabolic flux analysis in neurons utilizing a model that accounts for hexose phosphate recycling within the pentose phosphate pathway. *Neurochemistry international,* 93:26-39
23. Jekabsons, Mika et al. (2017). Updates to ^{13}C metabolic flux analysis model for evaluating energy metabolism in cultured cerebellar granule neurons from neonatal rats. *Neurochemistry International,* 109:54-67.
24. Dolfi, Sonia et al. (2013). The metabolic demands of cancer cells are coupled to their size and protein synthesis rates. *Cancer and Metabolism,* 1(1):1-20.
25. Berndt, Carsten., Lillig, Christopher., and Holmgren, Arne. (2007). Thiol-based mechanisms of the thioredoxin and glutaredoxin systems: implications for diseases in the cardiovascular system. *American Journal of Physiology-Heart and Circulatory Physiology,* 292(3):H1227-H1236.
26. Battin, Erin and Brumaghim, Julia. (2009). Antioxidant Activity of Sulfur and Selenium: A Review of Reactive Oxygen Species Scavenging, Glutathione Peroxidase, and Metal-Binding Antioxidant Mechanisms. *Cell Biochemistry and Biophysics,* 55(1):1-23.
27. Xiao, Zhiguang., La Fontaine, Sharon., Bush, Ashley., and Wedd, Anthony. (2018). Molecular Mechanisms of Glutaredoxin Enzymes: Versatile Hubs for Thiol-Disulfide Exchange between Protein Thiols and Glutathione. *Journal of Molecular Biology,* 431(2):158-177.
28. Lillig, Christopher, and Berndt, Carsten. (2013). Glutaredoxins in Thiol/Disulfide Exchange. *Antioxidants and Redox Signaling,* 18(13):1654-1665.
29. Calvert, Paula., Yao, Kang-Shen., Hamilton, Thomas., and O'Dwyer, Peter. (1998). Clinical studies of reversal of drug resistance based on glutathione. *Chemico-Biological Interactions,* 111-112:213-224.
30. Perry, Roger., Mazetta, Joann., Levin, Mark., and Barranco, Sam. (1993). Glutathione levels and variability in breast tumors and normal tissue. *Cancer,* 72(3):783-787.
31. Mattaini, Katherine., Sullivan, Mark., and Vander-Heiden, Matthew. (2016). The importance of serine metabolism in cancer. *Journal of Cell Biology,* 214(3):249-257.
32. Labuschagne, Christiaan et al. (2014). Serine, but Not Glycine, Supports One-Carbon Metabolism and Proliferation of Cancer Cells. *Cell Reports,* 7(4):1248-1258.
33. Locasale, Jason. (2013). Serine, glycine, and the one-carbon cycle: cancer metabolism in full circle. *Nature Reviews. Cancer,* 13(8):572-583.

34. Li, Albert et al. (2020). Metabolic Profiling Reveals a Dependency of Human Metastatic Breast Cancer on Mitochondrial Serine and One-Carbon Unit Metabolism. *Molecular Cancer Research,* 18(4):599-611.
35. Possemato, Richard et al. (2011). Functional genomics reveals serine synthesis is essential in PHGDH-amplified breast cancer. *Nature,* 476(7360):346-350.
36. Murphy, Patrick et al. (2018). The NAD+ Salvage Pathway Supports PHGDH-Driven Serine Biosynthesis. *Cell Reports,* 24(9):2381-2391.
37. Heinonen, Ilkka et al. (2013). Bone blood flow and metabolism in humans: Effect of muscular exercise and other physiological perturbations. *Journal of Bone and Mineral Research,* 28(5):1068-1074.
38. Pollari, Sirkku et al. (2011). Enhanced serine production by bone metastatic breast cancer cells stimulates osteoclastogenesis. *Breast Cancer Research and Treatment*, 125(2):421-430.
39. Ngo, Bryan et al. (2020). Limited Environmental Serine and Glycine Confer Brain Metastasis Sensitivity to PHGDH Inhibition. *Cancer Discovery,* 10(9):1352-1373.